

Studies on Marginally Trapped Tubes with Positive Cosmological Constant Λ

by

© *Haipeng Su*

A thesis submitted to the
School of Graduate Studies
in partial fulfilment of the
requirements for the degree of
Master of Science

Department of Physics and Physical Oceanography
Memorial University of Newfoundland

October 2019

St. John's

Newfoundland

Abstract

In general relativity, the cosmological constant Λ is a special term in the Einstein field equations. Many observational clues suggest that Λ is positive. In this thesis, we investigate the behavior of quasilocal horizons of black holes under the condition of positive Λ . We modify the $\Lambda = 0$ condition in [10] and recalculate the evolution of marginally trapped tube in Tolman-Bondi spacetime with non-vanishing Λ . Then, we apply the obtained results to some examples of the gravitational collapse of spherical dust clouds to investigate the influence of positive Λ on marginally trapped tube during the formation or growth of black hole. By analysis and comparison, we have found that there are significant effects of positive cosmological constant Λ on the behavior of marginally trapped tube evolutions in dust clouds collapse.

KEY WORDS : BLACK HOLE HORIZON, COSMOLOGICAL CONSTANT, EINSTEIN FIELD EQUATIONS, MARGINALLY TRAPPED TUBE, EVOLUTION PARAMETER, TOLMAN-BONDI SPACETIMES, DUST CLOUD.

Acknowledgements

First and foremost, I want to especially thank Dr. Ivan S. N. Booth, my supervisor, because without his ideas, support, guidance, and patience, this thesis would not be possible. Secondly, I want to express my gratitude to my wife, Dr. Jiao Zhang, and my parents for their encouragement and support in many aspects. Thirdly, I am deeply indebted to Dr. Tao Cheng, Dr. Jie Xiao and Mr. Afework Solomon for their guidance, encouragement and help. Moreover, I want to express my thanks and respects to Dr. Hari Krishna Kunduri, Dr. Martin Plumer and Dr. Qiyang Chen for their wonderful courses and teaching. Last but not least, I am very grateful to the Department of Physics and Physical Oceanography and the Department of Mathematics and Statistics in Memorial University for a good and free research environment. This study was partly supported by funding from Memorial University and NSERC.

Contents

Abstract	ii
Acknowledgements	iii
List of Symbols	vii
List of Abbreviations	viii
List of Tables	x
List of Figures	xi
1 Introduction	1
1.1 Overview	1
1.2 Thesis Outline	4
2 Boundaries of Black Holes	7
2.1 Classical Black Hole boundaries	7
2.1.1 Event Horizons	8
2.1.2 Killing Horizons	10

2.1.3	Trapped Surfaces	10
2.1.4	Apparent Horizons	12
2.2	Quasilocal Horizons of Black Holes	14
2.2.1	Trapping Horizons	15
2.2.2	Isolated Horizons	16
2.2.3	Dynamical Horizons	17
3	Mathematics of Spherically Symmetric Surfaces	19
3.1	Marginally Trapped Tube with Spherical Symmetry	20
3.1.1	General Properties of Marginally Trapped Tube	20
3.1.2	Evolution Parameter C with Nonzero Cosmological Constant Λ	22
3.1.3	Behaviors for Perfect Fluid	24
3.2	Tolman-Bondi Spacetimes with Positive Cosmological Constant Λ . .	26
4	Spherically Symmetric Dust Clouds Collapse	33
4.1	Collapse of Dust Ball	34
4.1.1	Collapse of the Dust Ball with Gaussian Initial Density	35
4.1.2	Oppenheimer-Snyder Collapse of Inhomogeneous Dust Ball . .	38
4.2	Accretion of Dust Shells onto the Pre-existing Black Holes	43
4.2.1	Small Dust Shell	44
4.2.2	Large Dust Shell	47
4.3	More Complicated Collapse	51
4.3.1	Multiple Spacelike Horizons	51
4.3.2	Multiple Timelike Membranes	55

5	Cosmological Horizons	60
5.1	Cosmological Horizons for the Collapse of Dust Ball	61
5.1.1	Collapse of the Dust Ball with Gaussian Initial Density	61
5.1.2	Oppenheimer-Snyder Collapse of Inhomogeneous Dust Ball	64
5.2	Cosmological Horizons for the Accretion of Dust Shells onto the Pre-existing Black Holes	67
5.2.1	Small Dust Shell	67
5.2.2	Large Dust Shell	72
5.3	Cosmological Horizons for More Complicated Collapse	75
5.3.1	Multiple Spacelike Horizons	75
5.3.2	Multiple Timelike Membranes	78
6	Conclusions and Future Studies	82
6.1	Conclusions and Discussions	82
6.2	Future Studies	85
	Bibliography	87
A	Classification of Black Holes	97
A.1	The Size of Black Holes	97
A.2	The Solutions of Black Holes	100
A.2.1	Schwarzschild Black Hole	100
A.2.2	Kerr Black Hole	105
A.2.3	Reissner-Nordström Black Hole	107
A.2.4	Summary	108

List of Symbols

Λ	Cosmological constant
M_{\odot}	Solar mass
r_s	Schwarzschild radius
J	Angular momentum
Q	Electric charge
l	Future-directed outgoing null normal vector field
n	Future-directed ingoing null normal vector field
$\theta_{(l)}$	Expansion of l
$\theta_{(n)}$	Expansion of n
T_{ab}	Stress-energy tensor
C	Evolution parameter

List of Abbreviations

MTT	Marginally trapped tube
EFE	Einstein field equation
Λ CDM	Λ -cold dark matter
EH	Event horizon
MTS	Marginally trapped surface
MOTS	Marginally outer trapped surface
MOTT	Marginally outer trapped tube
DH	Dynamical horizon
TLM	Timelike membrane
NEH	Non-expanding horizon
AH	Apparent horizon
IH	Isolated horizon
WIH	Weakly isolated horizon
TH	Trapping horizon
FOTH	Future outer trapping horizon

POTH Past outer trapping horizon
TBdS Tolman-Bondi-de Sitter
OS Oppenheimer-Snyder

List of Tables

A.1	Classification of black hole by size.	99
A.2	Classification of stationary black hole solutions of the Einstein-Maxwell equations by angular momentum and electric charge.	109

List of Figures

2.1	Kruskal diagram	9
2.2	Marginally trapped tube foliated by marginally trapped surfaces . . .	13
3.1	Penrose diagram of Tolman-Bondi-de Sitter spacetime	31
4.1	$\rho_0(r)$ vs r for a dust ball with Gaussian initial density	34
4.2	C vs r for the dust ball collapse	35
4.3	t vs R for MTT evolution in the dust ball collapse	37
4.4	$\rho_0(r)$ vs r for a dust ball in Oppenheimer-Snyder collapse	38
4.5	C vs r for the dust ball in Oppenheimer-Snyder collapse	41
4.6	t vs R for MTT evolution in Oppenheimer-Snyder collapse	42
4.7	$\rho_0(r)$ vs r for a small dust shell	44
4.8	C vs r for the small dust shell infalling	45
4.9	t vs R for MTT evolution in the small dust shell infalling	46
4.10	$\rho_0(r)$ vs r for a large dust shell with constant density	48
4.11	C vs r for the large dust shell infalling	49
4.12	t vs R for MTT evolution in the large dust shell infalling	50
4.13	$\rho_0(r)$ vs r for the multiple dust shells	52

4.14	C vs r for the multiple dust shells infalling	53
4.15	t vs R for MTT evolution in the multiple dust shells infalling	54
4.16	$\rho_0(r)$ vs r for the dust cloud in a more complicated collapse	56
4.17	C vs r for a more complicated collapse	57
4.18	t vs R for MTT evolution in a more complicated collapse	58
5.1	C vs r for the cosmological horizons in a dust ball collapse	62
5.2	t vs R for the cosmological horizon evolution in a dust ball collapse .	63
5.3	The cosmological and black hole horizons in a dust ball collapse . . .	65
5.4	C vs r for the cosmological horizons in Oppenheimer-Snyder collapse	66
5.5	The cosmological and black hole horizons in Oppenheimer-Snyder col- lapse	68
5.6	C vs r for the cosmological horizons in a small dust shell infalling . .	69
5.7	t vs R for the cosmological horizon evolution in a small dust shell infalling	70
5.8	The cosmological and black hole horizons in the dust shell infalling .	71
5.9	C vs r for the cosmological horizons in the large dust shell infalling .	72
5.10	t vs R for the cosmological horizons evolution in a large dust shell infalling	73
5.11	The cosmological and black hole horizons in a large dust shell infalling	74
5.12	C vs r for the multiple dust shells infalling	76
5.13	t vs R for the cosmological horizon evolution in the multiple dust shells infalling	77
5.14	The cosmological and black hole horizons in the multiple dust shells infalling	78

5.15	C vs r for a more complicated collapse	79
5.16	t vs R for the cosmological horizon evolution in a more complicated collapse	80
5.17	The cosmological and black hole horizons in a more complicated collapse	81
A.1	The First-ever Image of a Black Hole	98
A.2	Penrose diagram of Schwarzschild spacetime	102
A.3	Penrose diagram of Schwarzschild-de Sitter spacetime	103

Chapter 1

Introduction

1.1 Overview

Compact stars are a family of massive stellar objects with high density and small volume compared to their mass. Most compact stars are the remnants of stars after burning out their nuclear fuels¹. They are believed to be the endpoint of the stellar evolution process. There are three main types of compact stars: white dwarfs, neutron stars, and black holes [70]. If the mass of the compact star is higher than the upper limit of neutron stars, it would finally collapse into a black hole [83].

A black hole is the most interesting object found in our universe. In general, a black hole is a special region of spacetime with strong gravitational field from which it is impossible to send a signal from the inside out to infinity. At the center of this region, there should be a gravitational singularity with infinite density and curvature [80]. The theory of black holes is regarded as one of the most successful applications

¹Some compact stars (such as primordial black holes) might form during first-order phase transitions in the early Universe [47, 48].

of general relativity [61]. The Appendix A briefly introduces the classification of black holes by size and some other features.

Being independent but correlated with each other, the theoretical research into black holes can be divided into multiple branches [29, 30], such as black hole thermodynamics, black hole electrodynamics, black hole perturbation theory, black hole quantum physics, et cetera. However, in this thesis, we are interested in black hole horizons (especially quasilocal horizons) which are useful tools for the research on properties of black holes (We give a brief introduction to black hole horizons in Chapter 2).

In general relativity, the Einstein field equations (EFEs or Einstein's equations) play an important role in relating the spacetime curvature tensor to the density of mass-energy. In a spacetime $(M, g_{\mu\nu})$, the EFEs can be written as

$$R_{\mu\nu} - \frac{1}{2}Rg_{\mu\nu} + \Lambda g_{\mu\nu} = 8\pi T_{\mu\nu}, \quad (1.1)$$

where $T_{\mu\nu}$ is the stress-energy tensor of the present matter, $R_{\mu\nu}$ is the Ricci tensor associated with $g_{\mu\nu}$, R is the corresponding Ricci scalar, and Λ is the cosmological constant [18, 39, 61]. The EFEs provide us with a powerful tool to describe the gravitational effects of mass (or energy) on the spacetime.

In 1917, in order to obtain a static cosmological solution², Einstein first introduced the cosmological constant Λ into the EFEs (as the Equation (1.1)) to counteract the contraction caused by gravity [17, 66]. Therefore, the cosmological constant Λ can be considered as an anti-gravity effect which is associated with the vacuum energy

²This solution is also known as the “static Einstein universe” [10].

[17, 18, 57]

$$\rho_{\text{vac}} = \frac{\Lambda}{8\pi}, \quad (1.2)$$

where the ρ_{vac} is the vacuum energy density. In addition, the pressure corresponding to the vacuum energy can be expressed as $p_{\text{vac}} = -\rho_{\text{vac}}$ which is opposite in sign to cosmological constant [25, 71]. In the past century, the cosmological constant has greatly contributed to the development of cosmology (such as the age of the universe t_0 , dark energy, inflation, and Λ CDM³ model) [10]. Through the observations of the redshift of type Ia supernovae and galaxies, it is concluded that the expansion of our universe is accelerating [17]. Therefore, we can confirm that the cosmological constant is positive⁴ in our universe [85]. Moreover, it is not hard to predict that the density of matter will continue to decrease in this accelerating universe. Then, in the future, our universe will probably approach a de Sitter space⁵ in which the only form of energy is the vacuum energy associated with the positive cosmological constant [31, 40].

However, the presence of a cosmological constant has also led to many problems and debates. The most famous is the cosmological constant problem which is con-

³The “ Λ CDM” is the abbreviation of “ Λ -cold dark matter”.

⁴The Friedmann equations can be modified with nonzero cosmological constant [17], so the Equation (8.68) in [18] can be presented as

$$\frac{\ddot{a}}{a} = -\frac{4\pi}{3}(\rho + p) + \frac{\Lambda}{3}, \quad (1.3)$$

where $a(t)$ is the cosmic scale factor. If the cosmological constant Λ dominates in Equation (1.3), the \ddot{a} is positive which implies the accelerating expansion of the universe.

⁵In general relativity, the de Sitter space can be described as the maximally symmetric vacuum solution of EFEs with a positive cosmological constant Λ , while there is no other matter sources in this space [27, 31, 40].

sidered as a crisis of modern physics [17, 57]. In brief, the cosmological constant problem has been caused by the contradiction between the small value of cosmological constant⁶ and the quantum theoretical calculations⁷ [17, 57, 81]. Hence, this problem demonstrates that there are still some conflicts between general relativity and quantum field theory.

1.2 Thesis Outline

The main goal of this thesis is to study the effect of positive cosmological constant Λ on the evolution of black hole horizons. We extend the work of [10] to the positive Λ case. Hence, we calculate the geometric characteristics of marginally trapped tubes under spherically symmetrical conditions with nonzero Λ . Then, we apply the obtained results to several simple examples about the marginally trapped tubes associated with the spherical dust clouds in process of gravitational collapse⁸. We can analyse the influence of a positive Λ on marginally trapped tubes in this way. Unless we state otherwise, in this thesis, we have applied the system of units in which the speed of light c and gravitational constant G are both equal to one.

⁶In theory, cosmological constant can be expressed as [17, 57, 66]

$$\Lambda = 3\left(\frac{H_0}{c}\right)^2 \Omega_\Lambda, \quad (1.4)$$

where H_0 is Hubble's constant, Ω_Λ is the density parameter for cosmological constant, and c is the velocity of light in vacuum (We use units with $c = 1$ in other equations of this thesis). So the cosmological constant $\Lambda \approx 1.1059 \times 10^{-52} \text{m}^{-2}$. To simplify the discussion, the unit of Λ has been omitted from this thesis.

⁷The expectation for Λ exceeds the observational value by about 120 orders of magnitude [81].

⁸The formation or growth of black hole.

The rest of this thesis is organized as follows

Chapter 2 makes a brief overview of the traditional and quasilocal horizons of black holes. In particular we illustrate the problems of the global properties of classical black hole boundaries, so it is necessary to introduce the quasilocal horizons to describe the black hole boundaries.

In Chapter 3, we introduce some mathematical concepts and theorems of spherically symmetric horizons of black holes with nonzero cosmological constant Λ in general relativity. Firstly, we have reviewed the general features of marginally trapped tube with spherical symmetry. Then, the evolution parameter C is given to describe the evolutionary process of marginally trapped tubes. In addition, we have also made a brief introduction of the perfect fluid model in general relativity. Besides, we have presented the Tolman-Bondi spacetimes with positive cosmological constant Λ (Tolman-Bondi-de Sitter spacetimes) which can be used to study the gravitational collapse of spherically symmetric dust clouds.

In Chapter 4, we have applied the obtained results of the Chapter 3 to several examples⁹ about the formation or growth of a black hole during dust clouds collapse. In these examples, we have investigated the evolution of marginally trapped tubes in the gravitational collapse processes of the dust clouds under different conditions and compared the results of various cosmological constants. With these results, we can conclude the influences of these large positive cosmological constants on the behavior of marginally trapped tubes.

Chapter 5 makes extending study of the cosmological horizons which also appear in the process of dust clouds collapse with positive cosmological constant Λ . In the

⁹These examples have the same conditions as [10] except the nonzero cosmological constant Λ .

same examples of Chapter 4, we investigate the behaviors of the cosmological horizons in the formation or growth of black holes. In the evolution processes, the cosmological horizons always appear in the outside regions of black hole horizons, and they can shrink to the black horizons until these two kinds of horizons coincide.

Chapter 6 provides conclusions for this thesis and suggestions for future works.

Chapter 2

Boundaries of Black Holes

Over the past decades, black holes have been an important research area not only in general relativity but also in quantum mechanics and thermodynamics. Research on black holes can help us to understand some mathematical and physical concepts more deeply. In numerical relativity, the black hole boundary is an important object of study which is considered to reflect intrinsic features of black hole, such as singularity, mass, energy, and angular momentum [61].

2.1 Classical Black Hole boundaries

For the classical definition of a black hole in mathematics, we cannot identify the extent of a black hole just by locally defined characteristics. The region of black hole should be considered as a global property of the causal structure of a spacetime. However, for a distant observer, the formation of a black hole horizon should take infinite time because of the global nature [51]. In this section, we will review some classical definitions of black hole boundaries.

2.1.1 Event Horizons

In general relativity, a black hole in an asymptotically flat spacetime (M, g_{ab}) can be defined as the region from which no future-directed null geodesic can reach the future null infinity (\mathcal{I}^+) [76]. The boundary of black hole region is called event horizon (EH) and is a three-dimensional null hypersurface in M separating the points that are connected to infinity by a causal path from the points which are not [15]. The definition of event horizon is based on the global causal structure of the entire spacetime (M, g_{ab}) [9]. In four dimensions, the event horizon has topology $S^2 \times \mathfrak{R}$ and so be thought of as a three-dimensional tube in (M, g_{ab}) [27].

As shown in Figure 2.1, there are two $r = 2m$ surfaces in Schwarzschild spacetime. The surface separating Regions I and II is the future event horizon H^+ (the boundary of black hole), while the surface separating Regions I and III is the past event horizon H^- (the boundary of white hole). The event horizon of Schwarzschild black hole is stationary and spherically symmetric. For Kerr-Newman black hole introduced in Appendix A.2.2, the outer and inner event horizons are at $r_{\pm} = m \pm \sqrt{m^2 - a^2 - Q^2}$ [50, 78]. Moreover, in a universe with a positive cosmological constant Λ , the largest event horizon is called the de Sitter horizon and has radius $r = \sqrt{3/\Lambda}$ [31].

By Hawking's area theorem (the second law of black hole mechanics), if the weak energy condition holds, the area of an event horizon cannot decrease over time [80]. So it is impossible for a black hole to bifurcate or evaporate in classical general relativity¹. There are significant similarities between the area of black hole and the entropy in our universe. Moreover, for a rotating black hole (such as Kerr-Newman

¹However, the area theorem can be violated by considering the quantum effects [80].

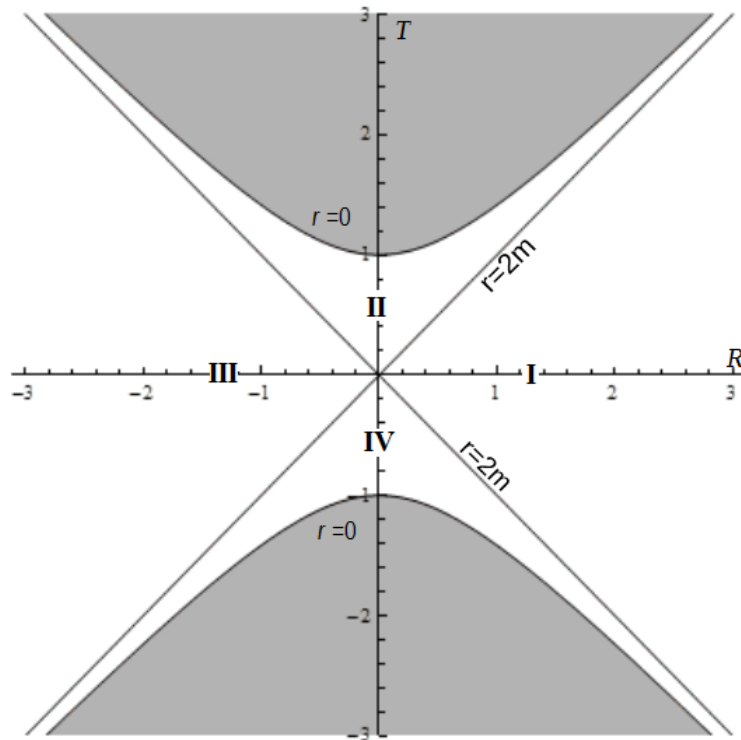


Figure 2.1: Kruskal diagram. Region I is our original universe. Region II presents the black hole. Region III describes the white hole. Region IV is the parallel universe which has properties identical with region I. $r = 0$ is the singularity [84].

black hole), the rotational energy between the event horizon and ergosphere can be extracted from black hole via the Penrose process [84].

2.1.2 Killing Horizons

For a smooth spacetime (M, g_{ab}) , a Killing vector field ξ^a generates a symmetry of this spacetime [27]. A Killing horizon H is defined as a three-dimensional null hypersurface of M which is tangent to a ξ^a everywhere, and the Killing vector field ξ^a is null ($\xi^a \xi_a = 0$) on H [9, 18, 27]. By the null condition of the Killing vector field ξ^a associated with the time symmetry, the event horizon and Killing horizon exactly coincide in a locally static spacetime (such as Schwarzschild black hole) [18, 27].

The Killing vector field ξ^a which is normal to H , satisfies a geodesic equation on Killing horizon H [18]

$$\xi^a \nabla_a \xi^b = \kappa \xi^b, \quad (2.1)$$

where κ is the surface gravity of H which contains intrinsic information about the spacetime. So a black hole can be defined by a Killing horizon with a surface area A and a surface gravity κ .

However, the Killing horizon ceases to be useful in the nonstationary spacetimes without timelike Killing vectors, because the Killing horizons cannot be defined in the situation of nonstationary spacetimes [27, 79].

2.1.3 Trapped Surfaces

Their global nature makes the identification of event horizons impractical for observers. By the singularity theorems in a spacetime, trapped surfaces can be used to

research the process of gravitational collapse to singularities [9, 18, 59].

In a connected four-dimensional spacetime (M, g_{ab}) , a trapped surface is defined as a closed, smooth, two-dimensional, connected spacelike submanifold with the sets of future-directed outgoing and ingoing null normal geodesics l and n ,² for which the expansion $\theta_{(l)}$ and $\theta_{(n)}$ are both negative everywhere³ [5, 9, 27, 80]:

$$\begin{cases} \theta_{(l)} = \tilde{q}^{ab} \nabla_a l_b < 0, \\ \theta_{(n)} = \tilde{q}^{ab} \nabla_a n_b < 0, \end{cases} \quad (2.2)$$

where the induced metric $\tilde{q}^{ab} = g_{ab} + l_a n_b + l_b n_a$ ⁴. Therefore, under the spherically symmetric condition, the light rays emitted from the trapped surface must converge in both the outgoing and ingoing directions [18, 27].

For this reason, in general relativity, identifying a trapped surface guarantees the existence of a spacetime singularity under appropriate energy conditions and some hypotheses [80]. In Schwarzschild spacetime, all points on any trapped surface must lie inside the event horizon of a black hole, and all spherical surfaces inside an extended

²We have normalized the l and n according to $l \cdot n = -1$ here (just like in Section 3.1.2).

³There is a more generalized definition of trapped surface: a compact, spacelike, two-dimensional surface on which $\theta_{(l)}\theta_{(n)} > 0$ [41, 42]. If $\theta_{(l)} > 0$ and $\theta_{(n)} > 0$, the trapped surface is past (anti-trapped surface) and refers to white hole; if $\theta_{(l)} < 0$ and $\theta_{(n)} < 0$, the trapped surface is future and corresponds to black hole [41].

⁴Compared with trapped surfaces, there are some other two-dimensional surfaces with different expansions [27]

- * Normal surface: $\theta_{(l)} > 0$ and $\theta_{(n)} < 0$;
- * Anti-trapped surface: $\theta_{(l)} > 0$ and $\theta_{(n)} > 0$;
- * Untrapped surface: the $\theta_{(l)}$ and $\theta_{(n)}$ are opposite in sign ($\theta_{(l)}\theta_{(n)} < 0$).

black hole are trapped surfaces [40, 80].

Further, for a closed, smooth, two-dimensional, connected spacelike submanifold S of M with the outgoing null expansion $\theta_{(l)} = 0$ [5, 9, 15]

- if the ingoing null expansion $\theta_{(n)} < 0$, then S is called a marginally trapped surface (MTS)⁵;
- if the ingoing null expansion $\theta_{(n)}$ is unrestricted, then S is known as a marginally outer trapped surface (MOTS)⁶.

Hence, there can be more than one MOTS in a spacelike slice.

Besides, as shown in Figure 2.2, a world tube T can be constructed by stacking up a family of MTSs with time evolving, this tube T is called a marginally trapped tube (MTT)⁷ [10, 68]. In general relativity, MTT can be classified as [10]

1. Dynamical horizon (DH) : MTT is spacelike everywhere.
2. Timelike membrane (TLM) : MTT is timelike everywhere.
3. Non-expanding horizon (NEH) : MTT is null everywhere.

2.1.4 Apparent Horizons

In a three-dimensional spacelike slice Σ , a MOTS can nest within other MOTS. The outermost MOTS of Σ is called an apparent horizon (AH) [9, 61]. An apparent horizon

⁵MTS is a kind of quasilocal horizon.

⁶Marginally outer trapped surface is also called marginal surface.

⁷MTT is also a type of quasilocal horizon, and we will particularly introduce the features of marginally trapped tube in Section 3.1.

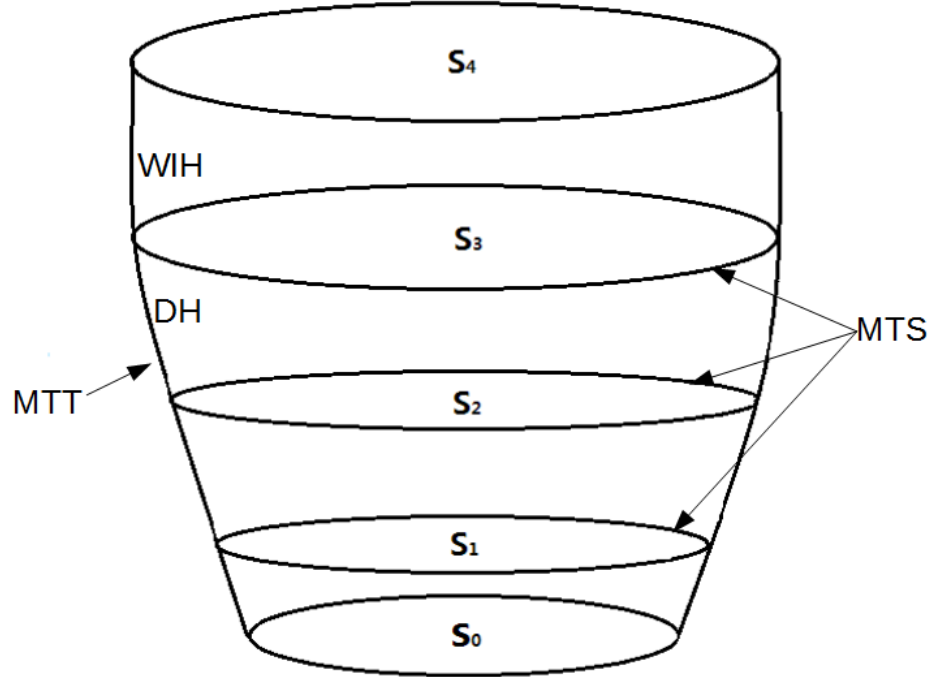


Figure 2.2: Marginally trapped tube (MTT) foliated by marginally trapped surfaces (MTSs) S_n . The expanding part of the hypersurface of MTT is dynamical horizon (DH), and the smooth part is weakly isolated horizon (WIH) [15].

can be defined as the outer boundary of a trapped region which is the collection of all the trapped surfaces in the slice Σ [61].

Comparing with event horizon, an apparent horizon of Σ can be defined locally in time, but non-locally in space [76]. Under the condition of $\theta_{(l)} = 0$, it is obvious that an apparent horizon can also coincide with event horizon in a stationary spacetime (like Schwarzschild spacetime) [61]. In this case, the apparent horizon of Σ can provide a useful approximation of the event horizon for numerical computations.

Thus, the apparent horizon can also be considered as an instantaneous boundary of black hole. However, in general, most apparent horizons are distinct from the event horizons for non-static spacetimes (like Vaidya spacetime) or the static black holes with perturbations [27, 61, 76]. Although most apparent horizons lie inside event horizons, some apparent horizons may be found outside of event horizons during the spherical collapse in non-Einstein gravity (such as Brans-Dicke gravity) [76].

Because apparent horizons are only local in time and solely confined to the slice Σ , they cannot completely substitute event horizons in general relativity [15]. The term of apparent horizon is also used to refer to the outermost surface with $\theta_{(l)} = 0$, it is a convenient method in practical applications (like numerical relativity) [9].

2.2 Quasilocal Horizons of Black Holes

From the above examples about the classical black hole horizons, we can find that the classical horizons work perfectly in stationary spacetimes. However, there are some problems for the classical notions in dynamical spacetimes because of the global property. It is inconvenient to evolve the whole spacetime when we need to localize horizons on some special hypersurfaces [62]. To solve the problems caused by the global property, researchers have to introduce the quasilocal approach to black hole boundaries [40]. Then, in the following decades, a great deal of progress has been made in research on quasilocal horizons which have the property of zero outgoing null expansion ($\theta_{(l)} = 0$). Now, the quasilocal horizon has already played an important role in general relativity, quantum gravity, and some other fields.

2.2.1 Trapping Horizons

In a four-dimensional spacetime (M, g_{ab}) , the three-dimensional boundary of the region which contains the trapped surfaces is called a trapping horizon (TH) [61]. It is a three-dimensional hypersurface of M foliated by a family of marginal surfaces which satisfy [27, 41]

$$\begin{cases} \theta_{(l)} = 0, \\ \theta_{(n)} \neq 0, \\ \mathcal{L}_n \theta_{(l)} \neq 0. \end{cases} \quad (2.3)$$

Equivalently, a MOTT can be considered as a trapping horizon while $\theta_{(n)} \neq 0$ and $\mathcal{L}_n \theta_{(l)} \neq 0$ [10].

Trapping horizon can be classified by the sign of $\theta_{(n)}$ and $\mathcal{L}_n \theta_{(l)}$ ⁸ [41, 42, 44, 62]

$$\begin{cases} \theta_{(n)} < 0, & \text{the trapping horizon is future ,} \\ \theta_{(n)} > 0, & \text{the trapping horizon is past ,} \end{cases} \quad (2.4)$$

and

$$\begin{cases} \mathcal{L}_n \theta_{(l)} < 0, & \text{the trapping horizon is outer ,} \\ \mathcal{L}_n \theta_{(l)} > 0, & \text{the trapping horizon is inner .} \end{cases} \quad (2.5)$$

According to the definitions above, the black hole boundary can be described by a future outer trapping horizon (FOTH), and the boundary of white hole can be considered as past outer trapping horizon (POTH) [41, 44].

The FOTH has particular significance in black hole thermodynamics, because the area of FOTH is associated with entropy of a black hole [27]. In general, a FOTH

⁸In some references, there are some variations in the definitions of the four types of trapping horizons, such as past outer trapping horizon ($\theta_{(n)} = 0$, $\theta_{(l)} > 0$, and $\mathcal{L}_l \theta_{(n)} < 0$) and past inner trapping horizon ($\theta_{(n)} = 0$, $\theta_{(l)} > 0$, and $\mathcal{L}_l \theta_{(n)} > 0$) [27, 44].

does not coincide with the event horizon, except in stationary spacetimes (such as the Kerr and Kerr-Newman family) [11, 27].

2.2.2 Isolated Horizons

As mentioned in Section 2.1.3, a non-expanding horizon (NEH) is a kind of marginally trapped tube which is null everywhere ($\theta_{(l)} = 0$ and $\theta_{(n)} < 0$ [27]). Hence, the NEH is the same thing as a null trapping horizon (future or past) [62]. More concretely, NEH can be defined as a three-dimensional null hypersurface Δ of a spacetime (M, g_{ab}) which satisfies [15, 26]

- this hypersurface Δ has a topology $S^2 \times \mathcal{R}$,
- the expansions $\theta_{(l)}$ of all null normal l^a of Δ have vanished,
- all motion equations hold on Δ ,
- for any future-directed null normal l^a , the $-T_a^b l^a$ is future-directed and causal (dominant energy condition).

The conditions above are local on Δ .

For a NEH Δ , $[l]$ is an equivalence class of the null normal l^a which satisfies [15]

$$[\mathcal{L}_l, \mathcal{D}_b]l^a = 0, \tag{2.6}$$

where \mathcal{D} is unique connection on Δ . Then, a weakly isolated horizon (WIH) is defined as the pair of $(\Delta, [l])$ [15, 26]. And the null normal l^a is a Killing vector of the intrinsic geometry of the Δ , without reference to the surroundings. Therefore, for the zeroth law holds on WIH $(\Delta, [l])$, the surface gravity κ_l is constant on $(\Delta, [l])$ [15]. The

restriction to WIH is not strict enough, so any NEH can be made into WIHs by identifying the corresponding equivalence class [6].

An isolated horizon (IH) can be defined as the WIH $(\Delta, [l])$ which all l^a of $[l]$ satisfy [26]

$$[\mathcal{L}_l, \mathcal{D}_b]v^a = 0, \quad (2.7)$$

where the v^a are arbitrary vector fields tangent to Δ .

Comparing with some other horizons, the isolated horizon framework is convenient for numerical relativity [4, 6]: unlike event horizon, IH is quasilocal; unlike Killing horizon, IH does not need to admit any Killing vectors in their neighborhood; and unlike apparent horizon, IH does not depend on the choice of spacelike slice. So the framework of IH has provided us with a way to model the equilibrium of black holes in time-dependent spacetime.

2.2.3 Dynamical Horizons

As mentioned in Section 2.1.3, dynamical horizon (DH) is considered as an expanding three-dimensional marginally trapped tube which is spacelike everywhere ($\theta_{(l)} = 0$ and $\theta_{(n)} < 0$)⁹. Equivalently, in a four-dimensional spacetime (M, g_{ab}) , a dynamical horizon can be defined as a three-dimensional, smooth, spacelike hypersurface H which is foliated by a family of compact two-dimensional marginally trapped surfaces S [49]. So the dynamical horizon is a spacelike future trapping horizon which can be used to make the quasilocal descriptions of evolving black holes by calculating mass and angular momentum [62].

⁹On the contrary, the shrinking MTT which is timelike everywhere is call a timelike membrane [5, 10, 27]. During evolution process, the TLM always shrinks while the DH always expands [10].

Under the condition of $\theta_{(n)} < 0$, the second law (area increase law) for black hole holds on a dynamical horizon¹⁰ [49]. For an evolving black hole, a DH is located in the region with time-dependent metric, and the DH can continuously expand until reaching equilibrium (evolving into WIH shown in Figure 2.2) [6]. The increase of the DH area is related to the energy flows and angular momentum crossed H which can be described by a set of flux laws, and the flux of energy is also related to the cosmological constant Λ [6]. We will discuss the situation of expanding DH in Chapter 3 and Chapter 4.

In a spacetime (M, g_{ab}) , it can be shown that the foliation of a dynamical horizon H by S must be unique in general [5]. For this DH, the past domain of dependence of $D^-(H)$ is defined as the set of all points p in M such that every future causal curve from them must intersect with the H [49]. So there is no DH which is completely located in the $D^-(H)$ [5].

¹⁰DH can only be crossed in one direction along causal curves [10].

Chapter 3

Mathematics of Spherically Symmetric Surfaces

To simplify the study of black hole boundaries, we assume the spacetime in this thesis to be spherically symmetric. For a spherically symmetric spacetime, orbits of the $SO(3)$ subgroup included in its isometry group are two-dimensional spheres [80]. These two-spheres are spacelike with constant positive Gaussian curvature [63]. In general relativity, spherical symmetry is also an important feature of many solutions for Einstein field equations, such as Schwarzschild solutions and Reissner-Nordström solutions.

3.1 Marginally Trapped Tube with Spherical Symmetry

3.1.1 General Properties of Marginally Trapped Tube

As mentioned in Section 2.1.3, a (future) marginally trapped tube¹ is defined as a smooth three-dimensional hypersurface in a four-dimensional spacetime (M, g_{ab}) which is foliated by a set of two-dimensional closed marginally trapped surfaces with $\theta_{(l)} = 0$ and $\theta_{(n)} < 0$ (shown as Figure 2.2) [10]. The family of MTSs referred to the leaves of foliation is obtained by time evolution [68]. In this way, they are marginally outer trapped tubes (MOTTs), while the foliated leaves are marginally outer trapped surfaces with only $\theta_{(l)} = 0$ and no condition on $\theta_{(n)}$ [3]. In the case of spherical symmetry, a spherical MTT is foliated by two-dimensional spherically symmetric MTSs.

In this research, we are interested in MTTs which are not null. As mentioned in Chapter 2, if the MTT is spacelike or timelike everywhere, it is called dynamical horizon or timelike membrane, respectively. Unlike DH, a TLM is not a one-way membrane, and it can be passed through by causal curves in both ingoing and outgoing directions [10]. Therefore, the second law of black hole mechanics is not suitable for TLM, and TLM always shrinks under the condition of $\theta_{(n)} < 0$ (TLM can also expand if $\theta_{(n)} > 0$) [68].

Due to spherical symmetry, the Einstein tensor G_{ab} and the stress-energy tensor T_{ab} can be simplified [56]. In Schwarzschild and Reissner-Nordström spacetimes, the

¹In some papers, marginally trapped tube is also known as holographic screen [36].

spherically symmetric MTT in general coincides with the EH of static black hole [82]. Moreover, in the process of a black hole expansion by matter falling in, if the mass density of the matter (like dust clouds) reaches a critical density ρ_c , a new horizon would appear in a nonzero region [10]. Hence, in Vaidya spacetimes with time-dependent mass, there are spherically symmetric solutions for Einstein field equations representing the gravitational collapse of infalling null dust [9, 10]. If the cosmological constant Λ is nonzero in this spacetime, a TLM will appear in the expanding black hole region with a DH [10]. And in Oppenheimer-Snyder spacetimes, TLM may also appear in the process of formation of black hole by spherical null dust clouds (like the results of Section 4.1.2) [10]. Moreover, the TLM inside the black hole may contract with infalling matter [9].

In this case, for the evolution of MTT, there can be TLM-DH pairs with the expanding DHs and the contracting TLMs in the collapse models with large concentration of matters (like the example of Section 4.3.2) [9, 10]. So in the process of formation or growth of the black hole with matter or radiation infalling, the DH expands firstly. While mass density is greater than a critical density ρ_c , TLM would appear in nonzero region. The new appeared TLM can shrink with the increasing density. This appearance of new horizon outside the old horizon in some extreme conditions can be called “horizon jumps” [10, 40]. In addition, the TLM-DH pairs can disappear while the shrinking TLMs vanish into singularities [10].

3.1.2 Evolution Parameter C with Nonzero Cosmological Constant Λ

For the spherically symmetric MTT with standard condition $l \cdot n = -1$, let a vector field \mathcal{V}^a be [10]

- tangent to the tube,
- orthogonal to the foliation MTSs everywhere,
- generating the foliation.

The vector field can be expressed as $\mathcal{V}^a = l^a - Cn^a$, where C is known as the evolution parameter². Because $\theta_{(l)} = 0$ on the horizon, we can get [9, 10]

$$\mathcal{L}_v \theta_{(l)} = \mathcal{L}_l \theta_{(l)} - C \mathcal{L}_n \theta_{(l)} = 0. \quad (3.1)$$

Thus, the function of C can be written as

$$C = \frac{\mathcal{L}_l \theta_{(l)}}{\mathcal{L}_n \theta_{(l)}}. \quad (3.2)$$

Under the conditions of $l \cdot n = -1$ and $l \cdot l = n \cdot n = 0$, there $\mathcal{V} \cdot \mathcal{V} = 2C$, so we can get the relations between C and MTT for $\theta_{(n)} < 0$ [9, 10, 23, 58]

- if $C > 0$, the MTT is spacelike and expanding as the DHs have appeared in this system;
- if $C = 0$, the MTT is null³ and constant area while there are IHs or null membranes for this tube;

² C is also called expansion parameter [9, 10].

³The MTT is also null while C is undefined (if $\mathcal{L}_l \theta_{(l)} \neq 0$ and $\mathcal{L}_n \theta_{(l)} = 0$). However, it is probably that the area of the null MTT under this condition is not constant.

- if $C < 0$, the MTT is timelike and contracting with TLMs.

Moreover, the sign of C depends on the sign of $\mathcal{L}_n\theta_{(l)}$, if the null energy condition⁴ holds [10].

In conditions of $\theta_{(n)} < 0$ and $\theta_{(l)} = 0$, we can get

$$\begin{cases} \mathcal{L}_l\theta_{(l)} = -4\pi\tilde{T}_{ab}l^al^b, \\ \mathcal{L}_n\theta_{(l)} = -1/(2R^2) + 4\pi\tilde{T}_{ab}l^an^b, \end{cases} \quad (3.5)$$

where

$$\tilde{T}_{ab} = T_{ab} - \rho_{\text{vac}}g_{ab} = T_{ab} - \frac{\Lambda}{8\pi}g_{ab}, \quad (3.6)$$

as the stress-energy tensor with the nonzero cosmological constant Λ in neutral condition⁵. Hence, Equation (3.2) can be evolved to

$$C = \frac{T_{ab}l^al^b}{(1/2A) - T_{ab}l^an^b - (\Lambda/8\pi)}, \quad (3.7)$$

where $A = 4\pi R^2$ is the area of the cross-section of MTT and R is the areal radius [10].

By comparing with Equation (2.3) in [10], the cosmological constant term is added to

⁴In general relativity, the null energy condition (NEC) states that the stress-energy tensor T_{ab} obeys

$$T_{ab}k^ak^b > 0, \quad (3.3)$$

where the k^a is an arbitrary future-directed null vector [65]. In this thesis, under the null energy condition, we have the Raychaudhuri equation

$$\frac{d\theta_{(l)}}{d\lambda} = -\frac{\theta_{(l)}^2}{2} - \sigma_{(l)ab}\sigma_{(l)}^{ab} - 8\pi T_{ab}l^al^b, \quad (3.4)$$

where λ is affine parameter for the null geodesics, and $\sigma_{(l)}$ is the shear. It is obvious that the first two terms on the right-hand side of Equation (3.4) are always non-positive. So under the null condition, we can get $\mathcal{L}_l\theta_{(l)} \leq 0$ [9, 10].

⁵In this thesis, \tilde{T}_{ab} can be seen as the stress-energy tensor of Tolman-Bondi-de Sitter spacetime.

Equation (3.7) of evolution parameter C , which is just like adding an extra pressure term to this system. Hence, the sign of C is associated with the absolute values of $(1/2A)$ and $((\Lambda/8\pi) + T_{ab}l^an^b)$. We can apply Equation (3.7) to some examples.

3.1.3 Behaviors for Perfect Fluid

If the fluid can be completely described by its isotropic pressure and mass density in its static frame, it is called perfect fluid. A perfect fluid cannot conduct heat or electric current and its viscosity vanishes [60]. In general relativity, there are spherically symmetric perfect fluid solutions for Einstein field equations in some isotropic coordinates [38].

The model of perfect fluid also depends on the four-velocity u^a which is a tangent vector field to the worldlines of the fluid particles. By the definition, the stress-energy tensor of a perfect fluid along timelike worldlines can be written as

$$T_{ab} = \rho u_a u_b + P(g_{ab} + u_a u_b), \quad (3.8)$$

where P is pressure of the fluid and ρ is the matter density of the fluid [10]. For some functions of ξ , the vector field u^a can be expressed as $u^a = \xi l^a + (2\xi)^{-1} n^a$, so we have

$$\begin{cases} u \cdot l = -1/(2\xi), \\ u \cdot n = -\xi. \end{cases} \quad (3.9)$$

P and ρ are related by the equation of state

$$P = w\rho, \quad (3.10)$$

where w is a constant independent of time [10, 18, 39]. Under the condition of positive

Λ , by Equations (3.8) and (3.9), Equation (3.7) can become

$$C = \frac{1}{2\xi^2} \frac{\rho + P}{(1/A) - (\rho + 3P) - (\Lambda/4\pi)} = \frac{1}{2\xi^2} \frac{(1+w)\rho}{(1/A) - (1+3w)\rho - (\Lambda/4\pi)}. \quad (3.11)$$

Thus, in general relativity, w and Λ term can determine the property of MTTs for the perfect fluid. By comparing with the result of zero cosmological constant⁶, we find that the critical value of w for which the MTT changes decreases (smaller than 1/3) in the presence of positive Λ .

In general, a pressureless perfect fluid is always called dust [61]. In a spherically symmetric dust-filled spacetime, the parameter $w = 0$ which is smaller than 1/3. Thus, the MTTs in the timelike perfect fluids are timelike and contracting [10]. In the dust-dominated case⁷, the equation of state of this system is $P = 0$, so that the stress-energy tensor in Equation (3.8) can be simplified to

$$T_{ab} = \rho u_a u_b. \quad (3.12)$$

Besides, Equation (3.11) can become

$$C = \frac{1}{2\xi^2} \frac{\rho}{(1/A) - \rho - (\Lambda/4\pi)}. \quad (3.13)$$

Hence, for the dust cloud as perfect fluid, the sign of C relies on the relative magnitude of $(\rho + (\Lambda/4\pi))$ and $1/A$. Obviously, the larger the positive cosmological constant Λ ,

⁶In [10], for $\Lambda = 0$, Dr. Booth pointed out that

- if $w < \frac{1}{3}$, MTTs are timelike and contracting;
- if $w = \frac{1}{3}$, MTTs are null and contracting;
- if $w > \frac{1}{3}$, MTTs are spacelike and expanding.

So 1/3 is the critical value of w for MTT with zero cosmological constant.

⁷The “dust” can be called “matter” in cosmology.

the greater of the evolution parameter C of the dust clouds, and there would be sign change of C when Λ is greater than a critical value⁸ (It will be shown in the results of Chapter 4).

3.2 Tolman-Bondi Spacetimes with Positive Cosmological Constant Λ

In the otherwise vacuum spacetimes, the gravitational collapse of null dust models with radial inhomogeneities and spherical symmetry can be described by the Tolman-Bondi (or Lemaitre-Tolman-Bondi) solutions. In comoving coordinates⁹, the spherically symmetric Tolman-Bondi metric can be written as

$$ds^2 = -dt^2 + \frac{(R'(t,r))^2}{1-k(r)}dr^2 + R^2(t,r)d\Omega^2, \quad (3.14)$$

where $k(r)$ is an arbitrary function of the coordinate radius r , $R(t,r)$ is the physical radius of the dust shell at proper time t , and $R'(t,r) = \partial R(t,r)/\partial r$ [10, 43]. The Tolman-Bondi spacetime with positive cosmological constant Λ is also known as Tolman-Bondi-de Sitter (TBdS) spacetime¹⁰ or Λ -LTB spacetime with the stress-energy tensor \tilde{T}_{ab} given by Equation (3.6) [33, 74].

In Tolman-Bondi spacetime, the proper time t is measured by the observers comoving with the dust clouds [9, 10]. For the spherically symmetric metric, some elements of the Einstein tensor and stress-energy tensor vanish, so the Einstein field

⁸The critical value depends mainly on the mass density ρ .

⁹The comoving coordinate is a Gaussian coordinate which comoves with the given dust clouds.

¹⁰If the Λ is negative, there is Tolman-Bondi-anti-de Sitter (TBAdS) spacetime.

equation (1.1) can be simplified to

$$\dot{R}^2(t, r) = \left(\frac{dR(r, t)}{dt} \right)^2 = \frac{2m(r)}{R(t, r)} - k(r) + \frac{\Lambda}{3} R^2(t, r), \quad (3.15a)$$

$$\dot{m}(r) = 0, \quad (3.15b)$$

$$\dot{k}(r) = 0, \quad (3.15c)$$

where $m(r)$ is the effective gravitational mass¹¹ inside the sphere of radius r , shown

$$m(r) = 4\pi \int_0^r \rho_0(\tilde{r}) \tilde{r}^2 d\tilde{r}. \quad (3.16)$$

Here $\rho_0(\tilde{r})$ is the matter density of the spherically symmetric dust cloud, and $k(r)$ is the determinant of gravitational boundedness of the matter system [10, 34, 43, 60]

$$k(r) = \frac{2m(r)}{r} - v_0^2(r), \quad (3.17)$$

with the initial areal velocity $v_0(r) = dr/dt$. For the initial condition $v_0(r) \leq 0$, all matter is initially stationary or infalling. In the Tolman-Bondi spacetime [34],

- for $k(r) < 0$, the system is gravitationally unbound;
- for $k(r) > 0$, the system is gravitationally bound;
- for $k(r) = 0$, the system is marginally bound.

In this study, we are interested in the effect of positive cosmological constant on the formation and growth of in dust cloud collapse. Hence, we have assumed that the

¹¹The effective gravitational mass $m(r)$ is not equal to the sum of masses of particles that formed the dust cloud.

system is marginally bound with $k(r) = 0$ [10]. For infalling process ($v_0(r) < 0$), Equation (3.15a) can be further simplified to

$$\dot{R}^2(t, r) = \frac{2m(r)}{R(t, r)} + \frac{\Lambda}{3}R^2(t, r). \quad (3.18)$$

In this case, there is an analytic solution of Equation (3.18) [10, 33, 60]

$$R(t, r) = \left(\frac{6m}{\Lambda}\right)^{\frac{1}{3}} \sinh^{\frac{2}{3}}\left(\frac{\sqrt{3\Lambda}}{2}[t_c(r) - t]\right), \quad (3.19)$$

where $t_c(r)$ is the proper time for complete collapse of a dust cloud with initial area radius $R(0, r)$ [28, 34, 35], and

$$t_c(r) = \frac{2}{\sqrt{3\Lambda}} \operatorname{arcsinh}\left(\sqrt{\frac{\Lambda r^3}{6m}}\right). \quad (3.20)$$

Hence, we can get the relevant derivatives of $R(t, r)$

$$R'(t, r) = \frac{dR(t, r)}{dr} = R(t, r) \left[\frac{m'}{3m} + \sqrt{\frac{\Lambda}{3}} t'_c(r) \coth\left(\frac{\sqrt{3\Lambda}}{2}[t_c(r) - t]\right) \right], \quad (3.21)$$

and

$$\dot{R}(t, r) = \frac{dR(t, r)}{dt} = -\sqrt{\frac{\Lambda}{3}} R(t, r) \coth\left(\frac{\sqrt{3\Lambda}}{2}[t_c(r) - t]\right), \quad (3.22)$$

where the negative sign refers to implosion [33, 34, 35].

In Tolman-Bondi spacetime, the expansions of the spherically symmetric MTSs are [9]

$$\theta_{(l)} = \frac{2(\dot{R}(t, r) + \sqrt{1 - k(r)})}{R(t, r)}, \quad (3.23)$$

and

$$\theta_{(n)} = \frac{\dot{R}(t, r) - \sqrt{1 - k(r)}}{R(t, r)}, \quad (3.24)$$

where $k(r) \leq 1$. Therefore, on the boundary of black hole where $\theta_{(l)} = 0$, by Equations (3.15a) and (3.23), we can get

$$R - 2m - \frac{\Lambda R^3}{3} = 0. \quad (3.25)$$

By direct calculation, there are three solutions of Equation (3.25)¹²

$$R_1 = -\frac{1}{2}\left(\frac{\Upsilon}{\Lambda} + \frac{1}{\Upsilon}\right) - i\frac{\sqrt{3}}{2}\left(\frac{\Upsilon}{\Lambda} - \frac{1}{\Upsilon}\right), \quad (3.27a)$$

$$R_2 = \frac{\Upsilon}{\Lambda} + \frac{1}{\Upsilon}, \quad (3.27b)$$

$$R_3 = -\frac{1}{2}\left(\frac{\Upsilon}{\Lambda} + \frac{1}{\Upsilon}\right) + i\frac{\sqrt{3}}{2}\left(\frac{\Upsilon}{\Lambda} - \frac{1}{\Upsilon}\right), \quad (3.27c)$$

where

$$\Upsilon = \left[(-3m + \sqrt{\frac{9m^2\Lambda - 1}{\Lambda}})\Lambda^2\right]^{\frac{1}{3}}, \quad (3.28)$$

and $3m\sqrt{\Lambda} < 1$ ¹³. It is obvious that R_3 is equal to $-(R_1 + R_2)$ which is unphysical because it is negative [33]. Moreover, when the positive Λ approaches zero, it is not hard to see that the dust cloud is transformed to the conditions in [10] as $R_1 = 2m$ and undefined R_2 . Equation (3.27a) corresponds to the apparent horizon of black hole, so $R_H = R_1$, where R_H is the areal radius R on the horizon. In addition, Equation (3.27b) refers to the cosmological horizon (or cosmological event horizon)¹⁴

¹²In [33, 35], there is another form of the solutions

$$R_1 = \frac{2}{\sqrt{\Lambda}} \sin\left[\frac{1}{3} \arcsin(3m\sqrt{\Lambda})\right], \quad (3.26a)$$

$$R_2 = \frac{2}{\sqrt{\Lambda}} \sin\left[\frac{1}{3} \arcsin(3m\sqrt{\Lambda}) + \frac{2\pi}{3}\right], \quad (3.26b)$$

$$R_3 = -R_1 - R_2, \quad (3.26c)$$

where $3m\sqrt{\Lambda} < 1$ and $R_2 > R_1$. Equations (3.26a), (3.26b) and (3.26c) are equivalent to our result (3.27a), (3.27b) and (3.27c), respectively. It is obvious that the equation forms of (3.26a) and (3.26b) are quite similar to Equation (A.10) in Schwarzschild-de Sitter spacetime.

¹³The imaginary bits in Equation (3.26a) can finally cancel out because $3m\sqrt{\Lambda} < 1$ in Equation (3.28).

¹⁴In general relativity, the cosmological horizon of an observer is the boundary of the region in which the observer can receive the signal from any points along the observer's worldline [63, 64]. We will discuss this situation in Chapter 5.

($R_2 > R_1$) [33, 34]. For the process of black hole formation with positive Λ , the black hole horizon appears and expands with the increasing mass, while the cosmological horizon shrinks due to the gravitational attraction of the black hole [7].

The Penrose diagram of Tolman-Bondi-de Sitter spacetime is similar to the case of Schwarzschild-de Sitter spacetime in Appendix A. In Figure 3.1, for the examples of Chapter 4 and Chapter 5, the behaviors of black hole horizons and cosmological horizons in the falling process are shown by the green dash line and the pink dot-dash line respectively. It is not hard to find that these two horizons would approach each other with increasing mass m and/or cosmological constant Λ . When the system reaches Nariai limit ($y = m^2\Lambda/3 = 1/27$), it would become a Nariai spacetime [13, 69].

For Equation (3.13), we take $\rho = \frac{1}{A} \frac{dm}{dR}$, $A = 4\pi R^2$ and $\xi = -1/2$, then the equation of the evolution parameter C can become

$$C = \frac{1}{2\xi^2} \frac{dm/dR}{1 - dm/dR - \Lambda R^2} = \frac{2dm/dr}{dR/dr - dm/dr - \Lambda R^2 dR/dr}, \quad (3.29)$$

where $dm/dR = (dm/dr)(dr/dR) = m'/R'$. Hence, on the black hole horizon, Equation (3.29) can be converted into

$$C_H = \frac{2m'}{R'_H - m' - \Lambda R_H^2 R'_H}. \quad (3.30)$$

Comparing to Equation (3.23) of [10], there is also a new Λ term in Equation (3.30) for evolution parameter C . Obviously, in Equation (3.30), the magnitude of Λ also plays a significant role for the sign of C . Therefore, we can assume that the behavior of the MTTs are related to the value of cosmological constant Λ . In Chapter 4, we have applied these obtained results to several examples about the formation and growth of

black holes in the process of dust clouds collapse under the extended conditions (the positive Λ case) of Section 3.3 in [10].

Chapter 4

Spherically Symmetric Dust Clouds Collapse

In this chapter, we investigate the influence of large positive cosmological constants¹ on the MTT evolutions in gravitational collapse of spherically symmetric dust clouds with various initial matter density $\rho_0(r)$ as in [10]. However, differing from [10], the dust cloud is infalling rather than initially stationary, so the initial areal velocity $v_0(r)$ is negative in our examples. In [10], Dr. Booth predicted that timelike membrane² would appear in this process while remaining a dynamical horizon (horizon jumps) in the presence of the nonzero cosmological constant Λ . By comparing with the results of [10], we find that the Λ term has significant effects on the MTT evolution which are basically correlated with the prediction in [10] about the influences of the nonzero cosmological constants on the formation and growth of black hole.

¹The cosmological constants with unit m^{-2} in Chapters 4 and 5 are significantly greater than the value from Equation (1.4).

²The TLM may be associated with the cosmological horizon discussed in Chapter 5 [10].

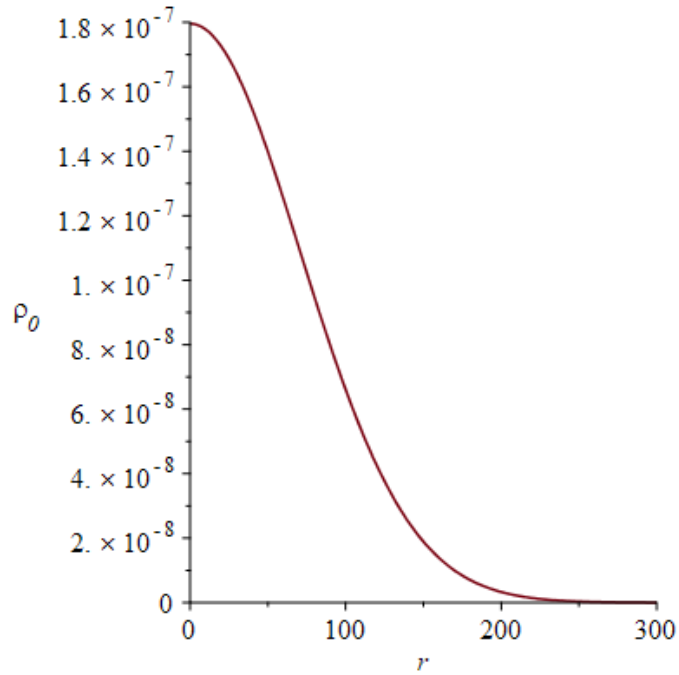


Figure 4.1: Collapse of a dust ball: $\rho_0(r)$ vs r .

4.1 Collapse of Dust Ball

In general relativity, studies of gravitational collapse of dust spheres have a long history. This collapse is related with the formation of black hole. During this collapse process, the initial mass density distribution of the dust balls plays an important role for the evolution of MTT [10]. In this section, we have researched two examples of dust ball collapse with positive cosmological constants which have significant effects on the results.

4.1.1 Collapse of the Dust Ball with Gaussian Initial Density

For a simple example of dust ball collapse, there is radial Gaussian distribution of initial mass density of a non-uniform dust sphere

$$\rho_0(r) = \frac{m_0}{\pi^{3/2}r_0^3}e^{-r^2/r_0^2}, \quad (4.1)$$

where m_0 is the total mass of this dust cloud³, and r_0 is the scale parameter. This distribution is shown in Figure 4.1 with $r_0 = 100m_0$, which r is plotted in units of m_0 while $\rho_0(r)$ is in units of m_0^{-2} [9, 10].

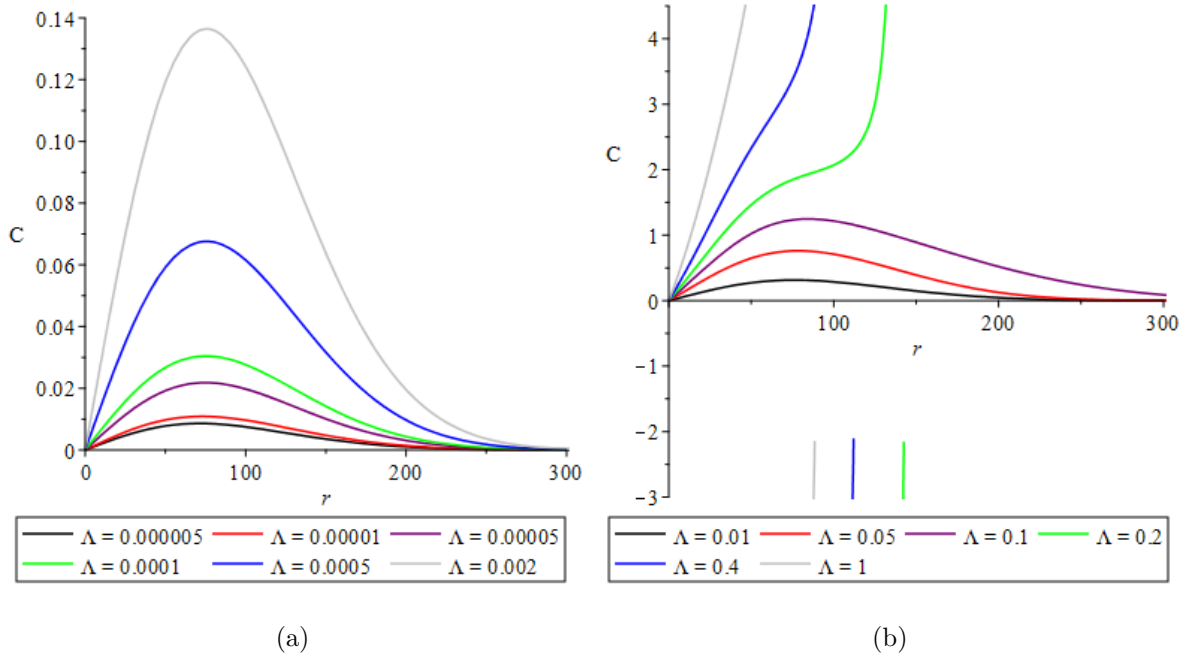


Figure 4.2: Collapse of a dust ball. (a) C vs r for relatively small positive cosmological constants. (b) C vs r for large positive cosmological constants.

As shown in Figures 4.2a and 4.2b, the curves refer to the evolution parameter C

³The m_0 corresponds to the $m(r)$ in Chapter 3.

with r . For relatively small Λ (approximately smaller than 0.11111), the curves of C are quite similar in shape to FIG.2b) in [10], and the peak values increase with the growing of Λ . However, for larger Λ , the curves of C are positive and also similar in shape to Figure 4.2a for small r , while the values of C become negative for large r . This means that a new MTT—timelike membrane appears in the region outside dynamical horizon in this collapse process⁴. This sign-alternating for C is related to the switch of $\mathcal{L}_n\theta_{(l)}$ with the increasing positive Λ [10]. In this way, the expanding DH and the shrinking TLM would finally merge with each other under the large positive cosmological constant condition. Moreover, the behavior of the black hole horizon with sign-alternating of C can be presented by the green line of the Penrose diagram in Figure 3.1.

Figure 4.3a describes the paths of the dust ball infalling by R in units of m_0 with proper time t . The initial points of MTT on the t axis represent t_c , the time of the dust shell falling into the zero area [10]. The shape of curves with relatively small Λ closely resembles the MTT evolution curve in FIG. 2c) of [10] with the same increasing region. Moreover, the curves also asymptotically approach the same vertical line ($R = 2m_0$) as [10], which indicates that this DH would finally approach a IH (as $t \rightarrow \infty$) [10].

As shown in Figure 4.3b, for the large Λ (approximately over 0.11111), the MTT curves are quite different from Figure 4.3a corresponding to the results in Figure 4.2. Hence, in the process of dust ball collapse with large positive Λ , a shrinking TLM firstly appears in the region around $R = 2m_0$, and after that a new expanding horizon (DH) appears at $R = 0$ (inside the timelike membrane). These two horizons finally

⁴This situation is consistent with the prediction in [10].

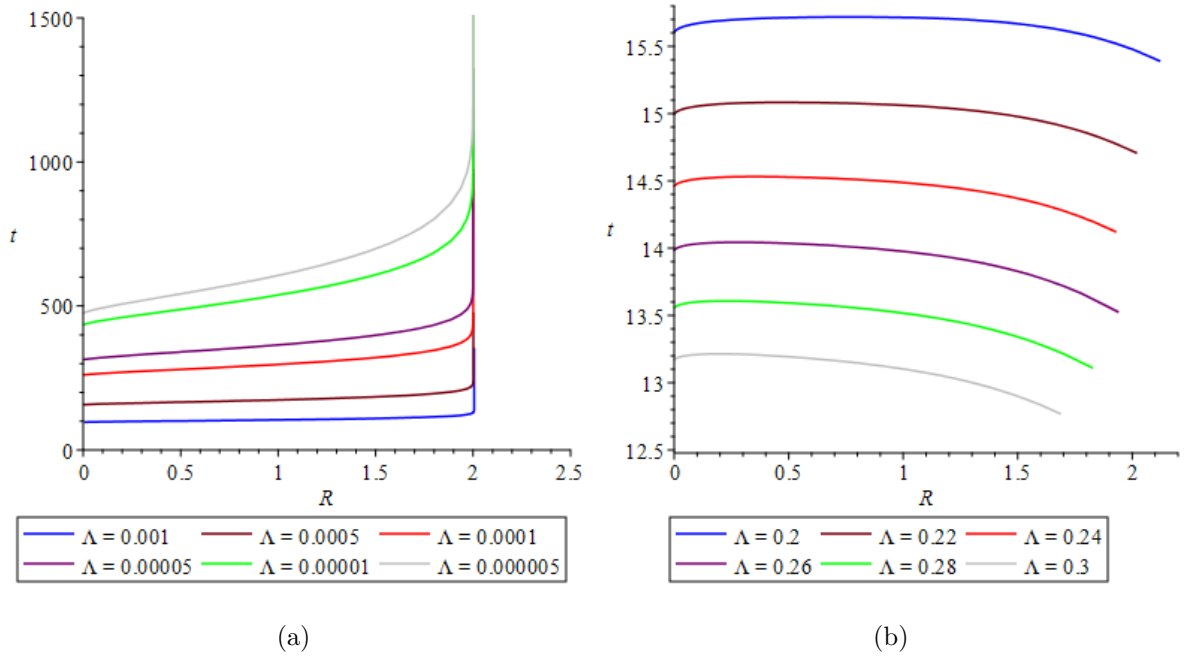


Figure 4.3: Collapse of a dust ball. (a) t vs R for MTT evolution with small positive cosmological constants. (b) t vs R for MTT evolution with large positive cosmological constants.

merge with each other in the collapse process over time⁵.

In addition, it is obvious that the smaller value of the Λ corresponds the longer time of the evolution process. Therefore, we can conclude that the positive cosmological constant can accelerate the formation of black hole in gravitational collapse of the dust ball with Gaussian distribution of initial mass density.

4.1.2 Oppenheimer-Snyder Collapse of Inhomogeneous Dust Ball

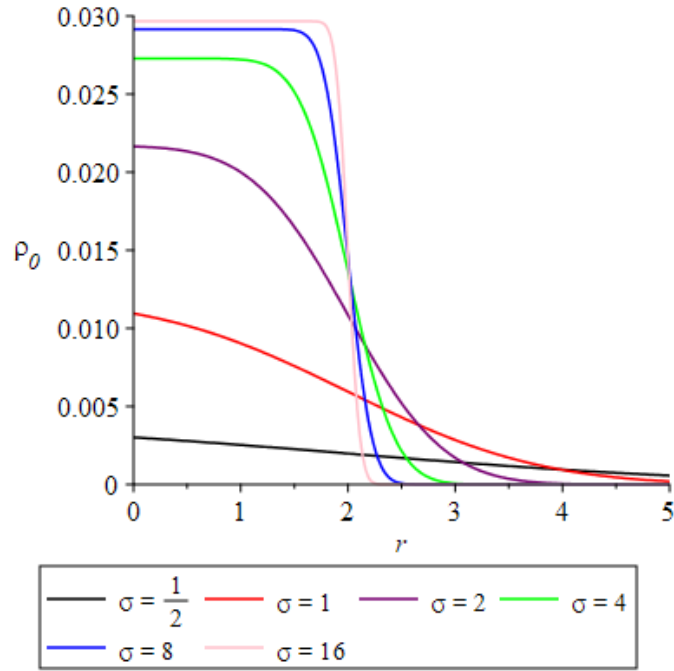


Figure 4.4: Oppenheimer-Snyder collapse: $\rho_0(r)$ vs r of the dust ball with various σ .

⁵By comparing with the results shown in Figure 5.2 and 5.3b, we have expected that the MTT of black hole with increasing positive Λ should asymptotically approach a cosmological horizon corresponding to the solution as Equation (3.27b). We will discuss this situation in Chapter 5.

The Oppenheimer-Snyder (OS) solution is a special case of Tolman-Bondi solutions for Einstein field equations. It can be used to describe the process of gravitational collapse of a non-rotating, spherically symmetric body into a black hole⁶. In the exterior of the dust clouds, the metric is the same as the Schwarzschild metric with Equation (A.1), while the metric inside the dust clouds can be expressed as [8, 61]

$$ds^2 = -dt^2 + a^2(t)(d\chi^2 + \sin^2\chi d\Omega^2), \quad (4.2)$$

where $\chi = \arcsin r$ and $a(t)$ is a scale factor which satisfies [8, 61]

$$\begin{cases} a(\eta) = \frac{1}{2}a_{\max}(1 + \cos \eta), \\ t(\eta) = \frac{1}{2}a_{\max}(\eta + \sin \eta), \end{cases} \quad (4.3)$$

where the a_{\max} is the maximum value of $a(t)$ and the η here is defined in $[0, \pi]$ (at the beginning of collapse $\eta = 0$, and $\eta = \pi$ at the end). The most significant feature of OS model is that it is completely analytic [46]. In this model, MTTs can be composed of unstable MTSs which are timelike or spacelike [8, 10]. For the positive cosmological constant condition, there are also Oppenheimer-Snyder-de Sitter (OSdS) spacetimes⁷ [53].

For the inhomogeneous dust ball, the initial mass density is

$$\rho_0(r) = \frac{m_0 F(\sigma)}{r_0^3} \left(1 - \operatorname{erf} \left[\sigma \left(\frac{r}{r_0} - 1 \right) \right] \right), \quad (4.4)$$

⁶In 1939, J. R. Oppenheimer and H. Snyder firstly used the OS spacetime to describe the gravitational collapse of homogeneous dust ball [61]. However, the dust ball in our example is inhomogeneous.

⁷By contrast, the Oppenheimer-Snyder-anti-de Sitter (OSAdS) spacetimes refer to the negative cosmological constant.

where $\text{erf}(x)$ is the error function, r_0 is the location of where $-d\rho/dr$ is the maximum value, σ represents the steepness of the step of r_0 , and $F(\sigma)$ is defined as [10]

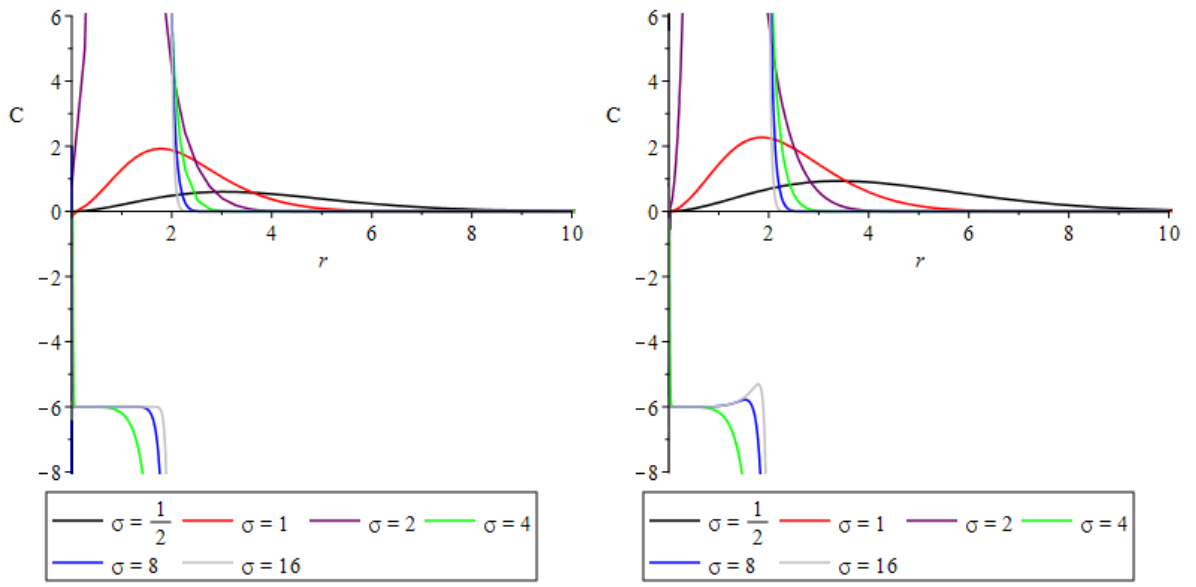
$$F(\sigma) = \frac{3\sigma^3}{2\pi\sigma(2\sigma^2 + 3)(1 + \text{erf}(\sigma)) + 4\sqrt{\pi}e^{-\sigma^2}(1 + \sigma^2)}. \quad (4.5)$$

In this example, we also choose $r_0 = 2m_0$ which makes m_0 to be the length scale. Then, in Figure 4.4 , the initial densities have become step functions with increasing σ which are identical with the FIG. 4a) of [10].

As shown in Figure 4.5a with $\Lambda = 0.0001$, it is obvious that the C curve for each σ is similar in shape to FIG. 4b) of [10]. This situation conforms to the behavior of black hole formation⁸ in OS spacetimes for the absence of the cosmological constant Λ in [10]. However, for $\Lambda = 0.05$, there are some slight differences in the shape of C curves with large σ (such as the small peaks on the curves of negative parts near the breaking points). Similar to the previous section, the peak values of C in FIG. 4b) of [10] are significantly smaller than Figure 4.2a and 4.2b with the same σ , so the larger Λ corresponds to the greater peak values. Moreover, if the value of positive Λ is greater than a critical value (about 0.111), there would be some significant difference on the curves of C . As shown in Figure 4.5c for $\Lambda = 0.5$, we have found that there are TLM-DH pairs corresponding to small σ (1/2, 1, and 2) , and there are only TLMs for large σ (4, 8, and 16).

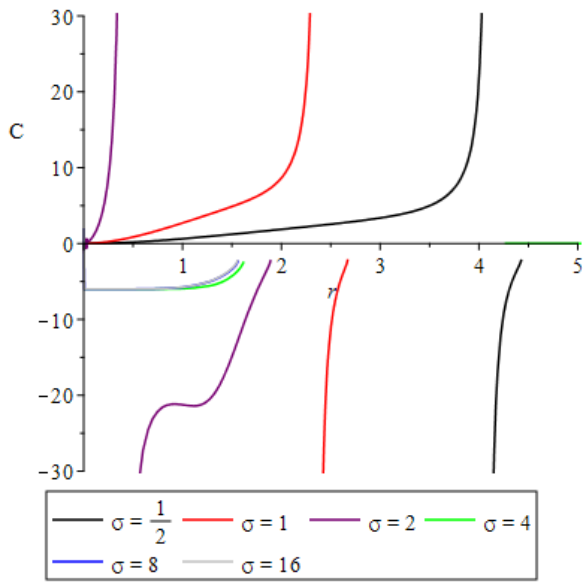
Figures 4.6a and 4.6b show the MTT evolution with $\Lambda = 0.0001$ and 0.05 respectively. Both of these figures are quite similar in shape to FIG. 4c) of [10]. We find that the dynamical horizons approach to $R = 2m_0$ in the case of $\Lambda < 0.001$ (such as Figure 4.6a), but the asymptotes become larger with the increasing cosmological

⁸The behavior is the appearance of DH-TLM pair in the collapse process.



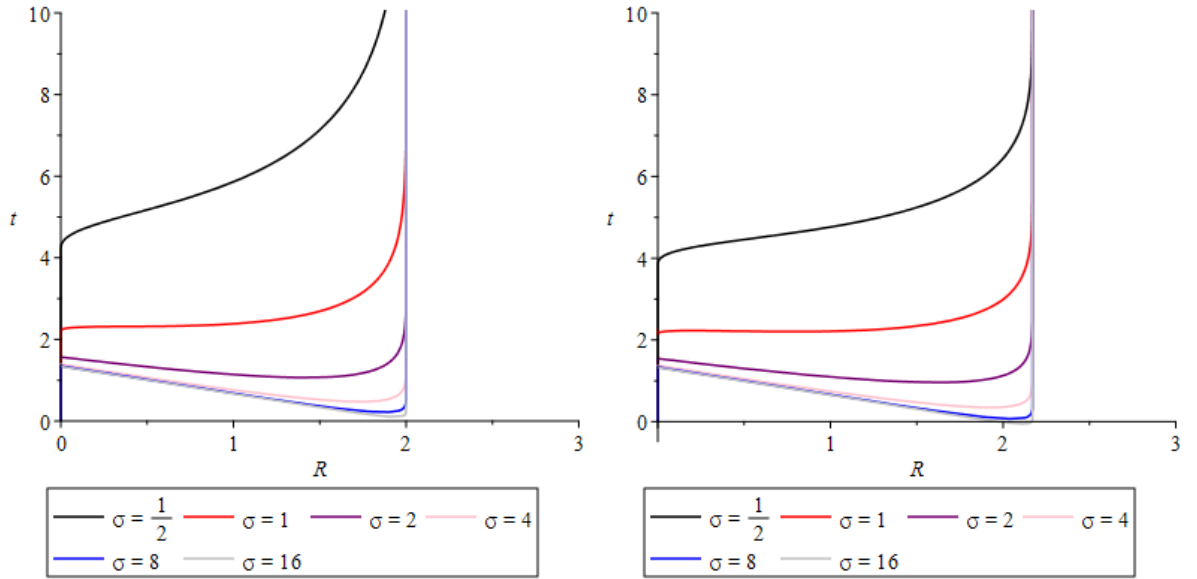
(a)

(b)



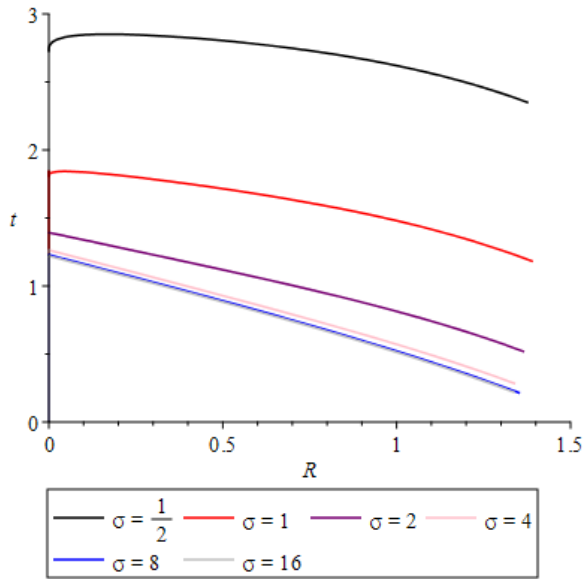
(c)

Figure 4.5: Oppenheimer-Snyder collapse. (a) C vs r for $\Lambda = 0.0001$. (b) C vs r for $\Lambda = 0.05$. (c) C vs r for $\Lambda = 0.5$



(a)

(b)



(c)

Figure 4.6: Oppenheimer-Snyder collapse. (a) t vs R for MTT evolution with $\Lambda = 0.0001$. (b) t vs R for MTT evolution with $\Lambda = 0.05$. (c) t vs R for MTT evolution with $\Lambda = 0.5$.

constant when $\Lambda > 0.001$. Besides, for large σ (greater than 2)⁹, the appearance time of the DH-TLM pair becomes earlier with the increasing Λ . Furthermore, the time of annihilation of TLM for large σ also significantly decreases with the growth of positive Λ . Resembling the result of Section 4.1.1, the MTT curves for small σ in Figure 4.6c show that a shrinking TLM would appear at beginning of the collapse, after then an expanding DH would appear too. They could even merge with each other over time. However, for large σ , there would be only a shrinking TLM in the collapse process referring to the result of Figure 4.5c.

By comparing with the results of different Λ in Figure 4.6, it is not hard to find that the formation of black hole can also be accelerated with positive cosmological constant in Oppenheimer-Snyder collapse.

4.2 Accretion of Dust Shells onto the Pre-existing Black Holes

Following the examples of dust spheres, we have investigated the accretion of dust shells onto the pre-existing black holes in the presence of positive cosmological constant Λ . For the dust shell onto a pre-existing black hole, the metric in the inner region of this shell is time-dependent and influenced by the properties of this dust shell [52].

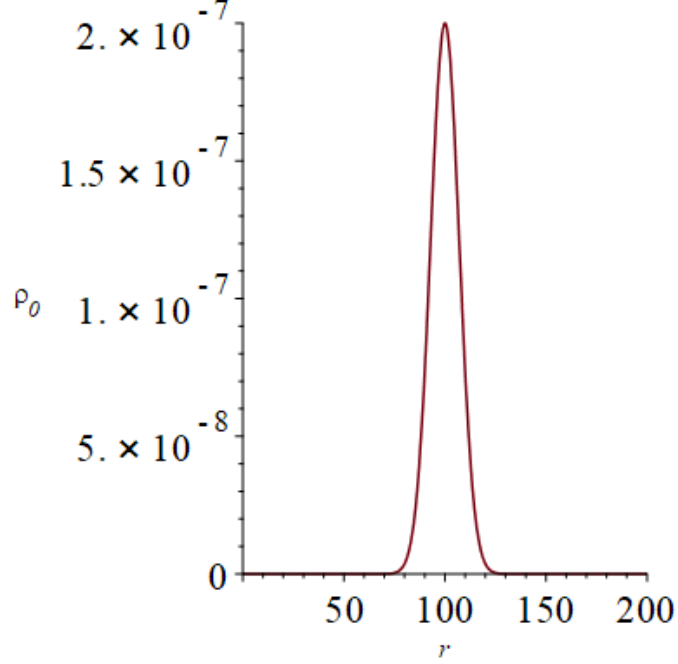


Figure 4.7: Small dust shell: $\rho_0(r)$ vs r .

4.2.1 Small Dust Shell

For a spherical dust shell, the initial mass density can be written by the Gaussian distribution

$$\rho_0(r) = \frac{m_0}{2\pi^{3/2}r_0^3(2\alpha^2 + 1)} e^{-\left(\frac{r}{r_0} - \alpha\right)^2}, \quad (4.6)$$

where m_0 is the total mass of the dust shell, r_0 represents the thickness of the shell, and α characterizes the initial position of the shell in terms of r_0 [10]. It is obvious that there is a peak of this density $\rho_0(r)$ at $r = \alpha r_0$ as the radius of the shell. In this example, we have ignored the small region in the interior of the shell spacetime and described the inner spacetime as a Schwarzschild geometry with mass M . In this

⁹For small value of σ , the MTT curves continuously increase as in the case of zero Λ .

way, there is the mass function of this system

$$m(r) = M + 4\pi \int_{r_j}^r \rho_0(\tilde{r}) \tilde{r}^2 d\tilde{r}, \quad (4.7)$$

where the r_j is the position of the junction of the shell and the inner spacetime.

In Figure 4.7, we take M as the length scale, and choose $m_0 = M/2$, $r_0 = 10M$, $\alpha = 10$, and $r_j = 2.5M$. So we get the curve of $\rho_0(r)$ with the peak at $r = 100M$ which is exactly the same as the FIG. 5a) in [10].

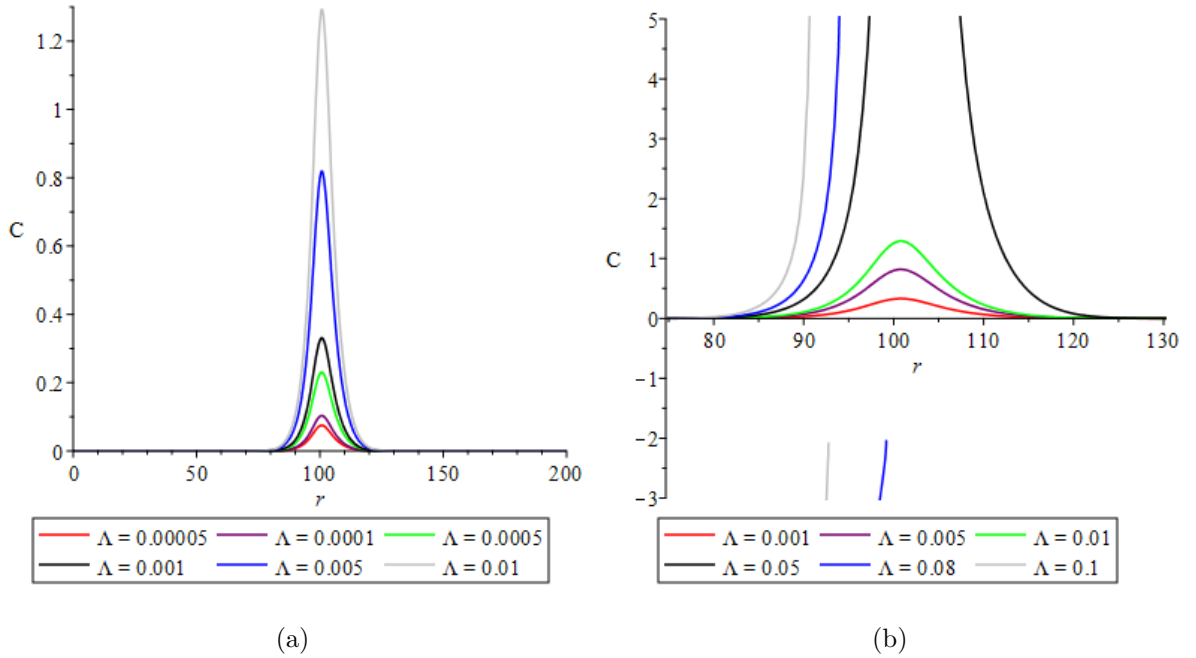


Figure 4.8: Small dust shell. (a) C vs r for small positive cosmological constants. (b) C vs r for large positive cosmological constants.

Similar to the examples of Section 4.1, we find that the shape of C curves with small Λ (approximately smaller than 0.052) in Figure 4.8 resembles FIG. 5b) of [10]. However, for the Λ in a small range around 0.052, the top of peak is shifted to the

negative C quadrant of this coordinate¹⁰ (similar to the situation of C curves in Section 4.3.2). Then, the shape of C curves with large Λ is similar to the curves of Figure 4.8a for small r , but the C curve becomes negative for large r which also indicates the appearance of TLM in that region. Hence, there can be TLM-DH pairs when the positive Λ is greater than a critical value (about 0.052). Therefore, this situation also corresponds to the prediction in [10].

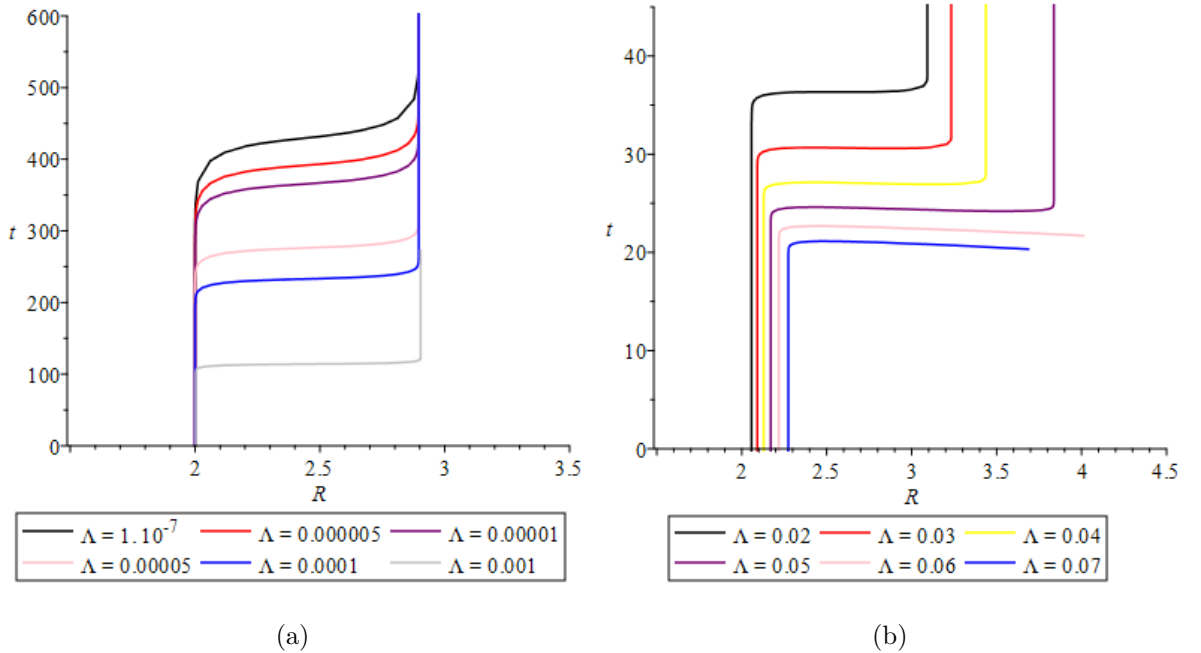


Figure 4.9: Small dust shell. (a) t vs R for MTT evolution with small positive cosmological constants. (b) t vs R for MTT evolution with large positive cosmological constants.

Obviously, in Figure 4.9a, the curves of MTT evolution for small positive Λ are also similar to FIG. 5c) in [10] with the same asymptote for the IH near $R = 3M$.

¹⁰The value of C at the peak is smaller than about -3350 which cannot be shown in Figure 4.8b.

The curve of MTT evolution for such small positive Λ increases continuously as [10]. However, the turning points of these curves become lower with the rise of positive Λ . This situation indicates that the DH can also approach to the IH at $R = 3M$ earlier with the smaller Λ .

However, Figure 4.9b shows that the shape of MTT evolution curves with large positive Λ is significantly different from Figure 4.9a (but it is quite similar to FIG.7c) in [10]). Corresponding to the situation of TLM's appearance shown in Figure 4.8b, it can be seen from the curve that new horizon appears and divides into DH and TLM in the region outside the original horizon (DH), while the mass density increases to a critical value. The new DH can quickly approach the IH, and the new shrinking TLM can merge with the old expanding DH over time. In addition, while Λ is greater than a critical value (about 0.052), the new expanding DH would not appear in this evolving process. This situation is quite similar to the results of previous sections which will be related with the behaviors of cosmological horizons in Chapter 5.

Comparing with the MTT evolution curves of various positive cosmological constants, as the conclusions of previous sections, the positive cosmological constant can also accelerate the growth of black hole during the infalling process of the small dust shell with Gaussian initial density.

4.2.2 Large Dust Shell

For a thick uniform dust shell with spherical symmetry, the initial mass density takes the form

$$\rho_0(r) = \frac{3m_0 \left(\operatorname{erf}\left(\frac{r-r_1}{M}\right) - \operatorname{erf}\left(\frac{r-r_2}{M}\right) \right)}{4\pi(r_2 - r_1)(2r_1^2 + 2r_1r_2 + 2r_2^2 + 3M^2)}, \quad (4.8)$$

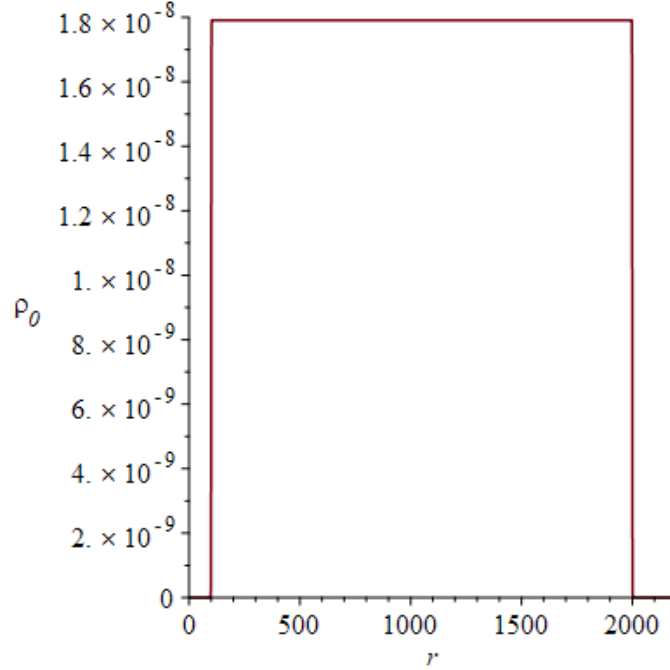


Figure 4.10: Large dust shell: $\rho_0(r)$ vs r .

where m_0 is the total mass of the dust shell, r_1 and r_2 are the approximate starting and stopping points of the shell respectively, and M is the mass of the pre-existing black hole [10]. Hence, the full mass function of the system with large dust shell is the same as Equation (4.7) in form.

Taking $m_0 = 600M$, $r_1 = 100M$, and $r_2 = 2000M$ in this example with the length scale M , we can get Figure 4.10 for the initial mass density $\rho_0(r)$ of the large dust shell as [10]. It is obvious that the density $\rho_0(r)$ is approximately constant between r_1 and r_2 inside the shell.

In accord with the previous sections, the curve of C with $\Lambda = 1 \times 10^{-7}$ shown in Figure 4.11a is almost the same as the FIG. 7b) of [10] with the negative part for large r . Moreover, the Figure 4.11b indicates that for several positive cosmological

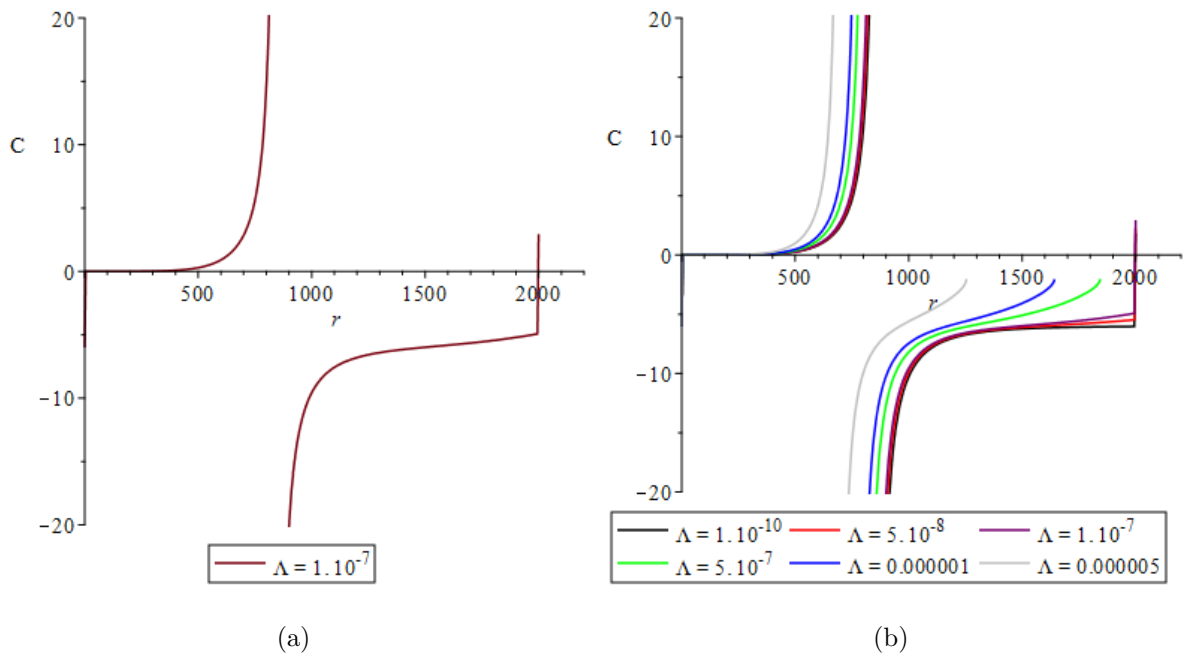


Figure 4.11: Large dust shell. (a) C vs r for $\Lambda = 1 \times 10^{-7}$. (b) C vs r for various positive cosmological constants.

constants, C curves have roughly the same shape, but the r value of the breaking point on C curve is becoming smaller with the increasing Λ . Besides, it is not hard for us to find that the C curves disappear in large r while the cosmological constant is approximately greater than 3×10^{-7} .

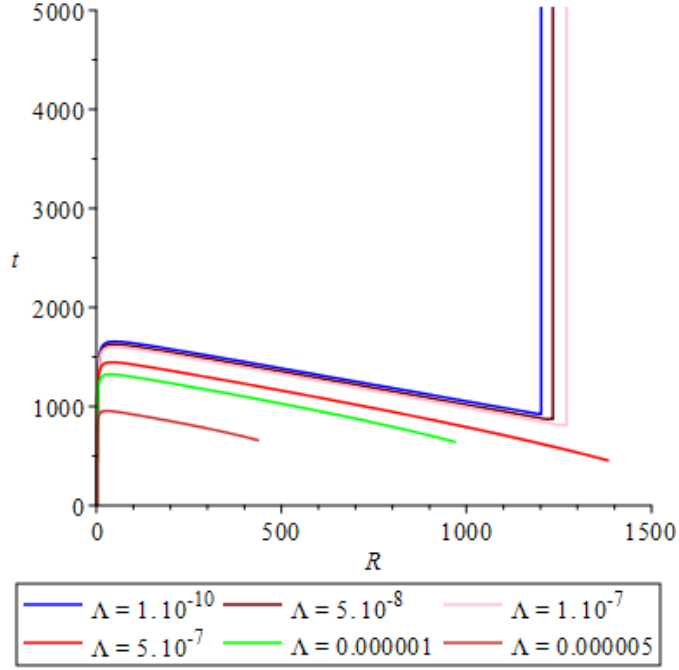


Figure 4.12: Large dust shell: t vs R for MTT evolution with various positive cosmological constants.

As shown in Figure 4.12, for relatively small positive Λ , the curves of MTT evolutions as the functions of R are also affected by Λ terms. The shapes of the MTT evolution curves resemble FIG. 7c) in [10], which indicate that the new horizon can also appear and bifurcate into DH and TLM in the presence of positive cosmological constant. By the rise of positive Λ , the time of the new MTS appearance is significantly earlier, and the radius of IH (asymptote) becomes larger. Therefore, we can

also conclude that the process of MTT evolution for large dust shell can also be accelerated by the positive Λ (as the results of previous sections). Moreover, if positive Λ is greater than critical value (approximate 3×10^{-7}), the new horizon would not divide after appearance, instead it would contract continuously until merging with the original horizon.

4.3 More Complicated Collapse

Following the previous examples of the dust clouds collapse in the presence of positive cosmological constant Λ , we have studied two more complicated examples of collapse in this section. Comparing with the two examples in Section 3.5 of [10] which considered the cases of spacelike and timelike respectively, there are some obvious differences in our results under the condition of $\Lambda > 0$.

4.3.1 Multiple Spacelike Horizons

For a spherically symmetric dust cloud with multiple shells, the distribution of mass density is

$$\rho_0(r) = \frac{\alpha\mu}{2\pi^2 r_0 r^2} \sin^2\left(\alpha \frac{r}{r_0}\right), \quad (4.9)$$

where r_0 is an arbitrary reference length scale, and μ is the mass of shell between $r = N\pi r_0/\alpha$ and $r = (N + 1)\pi r_0/\alpha$ with the positive integer N . We can find that each of the series of shells has the same mass due to the decreasing density $\rho_0(r)$ [10]. To avoid the cases of shell crossings and initial black holes, we have chosen that $\mu = (8\pi/5)r_0$ and $\alpha = 1/4$. Thus, the distribution of density ρ_0 shown in Figure 4.13 is identical with the FIG. 8a) of [10].

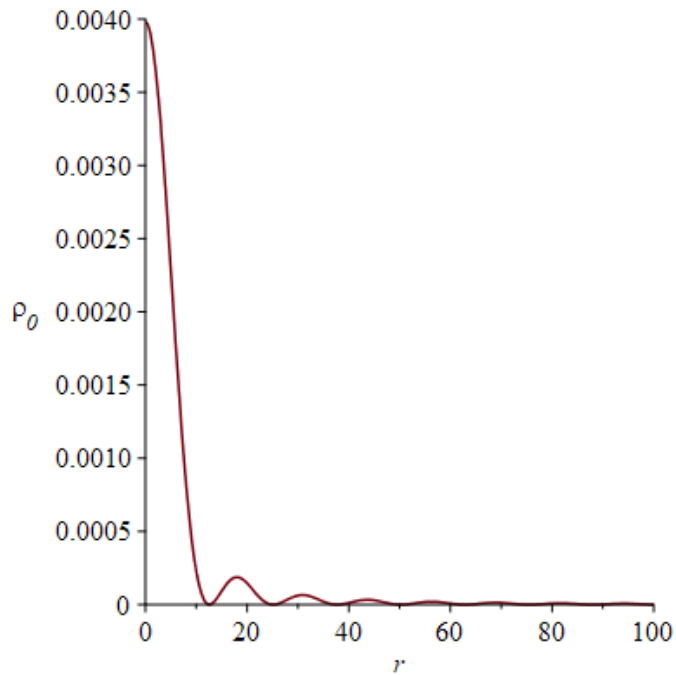


Figure 4.13: Multiple dust shells fall into a black hole: $\rho_0(r)$ vs r of the dust shells.

It can be seen that the shapes of the C curves in Figure 4.14a for $\Lambda = 1 \times 10^{-8}$ and Figure 4.14b for $\Lambda = 1 \times 10^{-7}$ and 1×10^{-5} all resemble to the C curve of FIG. 8b) in [10], which means that the MTT is also either spacelike or null everywhere in case of small positive cosmological constants (approximately smaller than 2×10^{-5}) in the range of $0 < r < 100r_0$.

However, in Figure 4.14b, with the increasing Λ , the top parts of some peaks change to negative. Thus, the MTT can alternate between spacelike and timelike for large positive Λ corresponding to the appearance of TLM-DH pairs in the radius range of $0 - 100r_0$. This situation is similar to the result of Section 3.5.2 in [10], while the appearance of TLM-DH pairs with the large positive cosmological constants is also consistent with the prediction of [10].

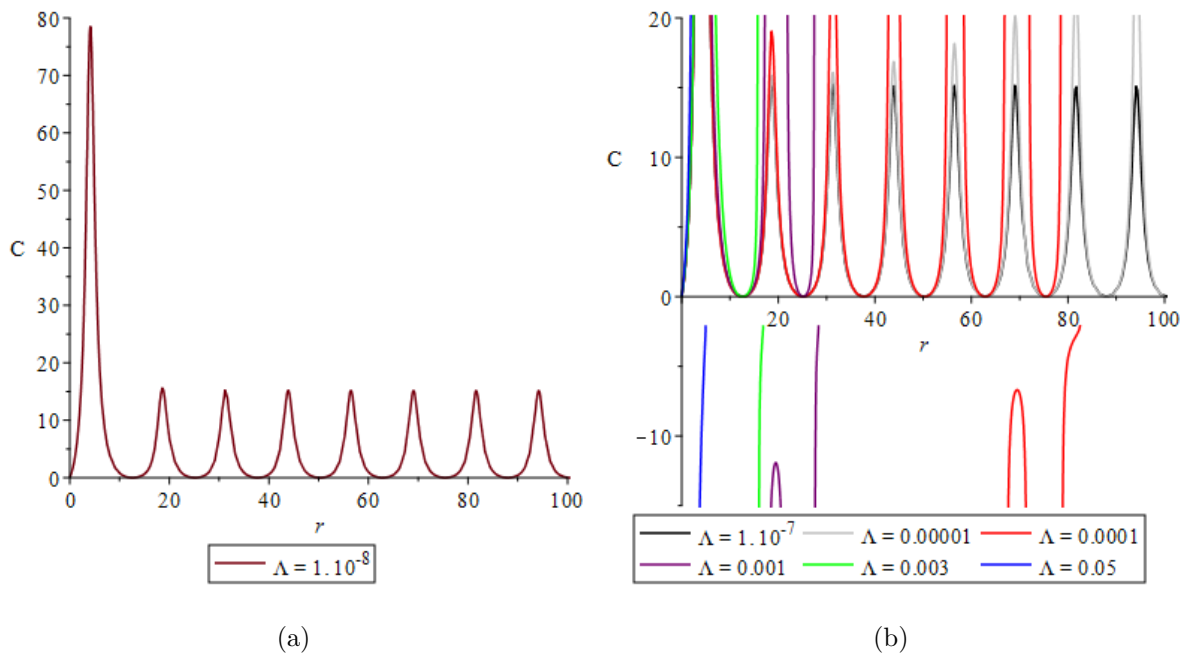


Figure 4.14: Multiple dust shells fall into a black hole. (a) C vs r for $\Lambda = 1 \times 10^{-8}$.

(b) C vs r for various positive cosmological constants.

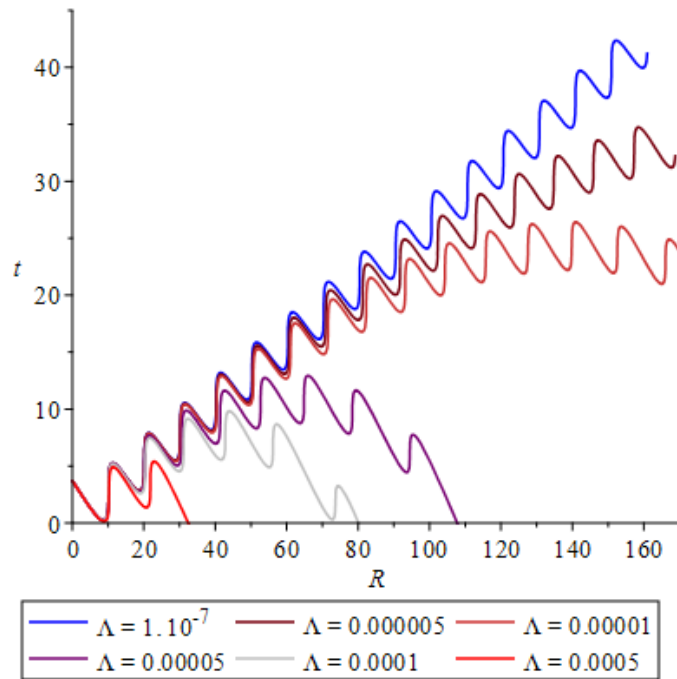


Figure 4.15: Multiple dust shells fall into a black hole: t vs R for MTT evolution with various positive cosmological constants.

As shown in Figure 4.15, the curves of MTT evolution with positive cosmological constants are also similar in shapes to FIG. 8c) in [10]. The wavy structure of the curves corresponds to the structure of dust density ρ_0 . In [10], there can be one to four MTSs in the t =constant surfaces. However, we find that the MTT curves bend to the R -axis (like a “semi-circle” with wavy boundaries) which may manifest that the t =constant surfaces can contain more than four MTSs due to the positive cosmological constants¹¹. It is obvious that the “radii” of the “semi-circles” become shorter with the increasing positive Λ . This behavior also corresponds to the acceleration of the MTT evolution in the presence of positive cosmological constant Λ . The MTT evolution curve can be considered as a sequence of units similar to the case in Figure 4.12, and the mode of the MTT evolution in each unit is also like the Section 4.2.2. So there are more “horizon jumps” under this condition, which means more new horizons can appear and evolve¹² in some external regions.

4.3.2 Multiple Timelike Membranes

For the MTT which is composed of multiple DH and TLM regions, the mass density of the dust cloud can be expressed as

$$\rho_0(r) = \begin{cases} \frac{\alpha}{r_0^2} \left[\pi - \frac{r}{5r_0} \left(2 \cos^2 \left(5 \frac{r}{r_0} \right) + 3 \right) \right], & 0 \leq r \leq \pi r_0, \\ 0, & r > \pi r_0, \end{cases} \quad (4.10)$$

where α is a dimensionless constant [10]. For the case of $r > \pi r_0$, the spacetime is Schwarzschild with mass $M = m(\pi r_0)$ [10]. To avoid shell-crossings and initial black

¹¹There are also cosmological horizons corresponding to each black hole horizons which will be discussed in Chapter 5.

¹²These new horizons can also bifurcate and annihilate over time.

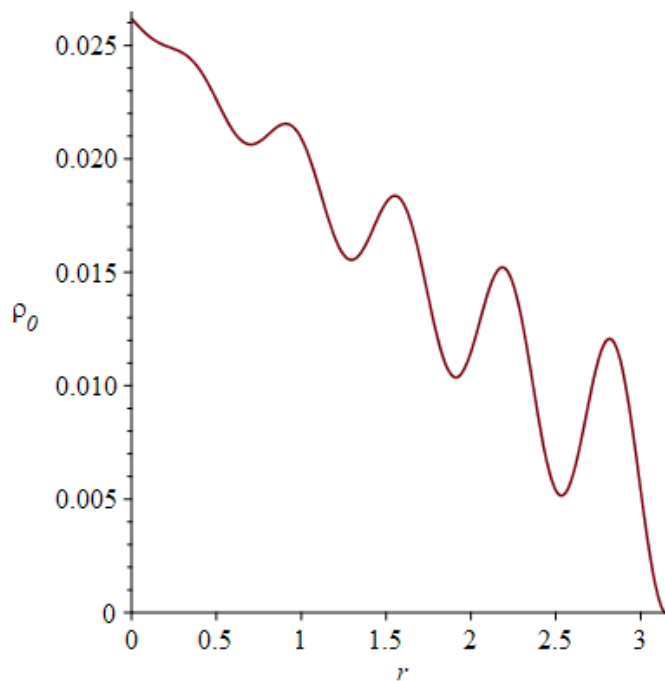


Figure 4.16: A more complicated collapse: $\rho_0(r)$ vs r of the dust cloud.

holes in this spacetime, we have chosen $\alpha = 1/120$. Hence, with the length scale r_0 , the mass density $\rho_0(r)$ is shown in Figure 4.16 which indicates multiple shells of the dust cloud.

Obviously, as shown in Figure 4.17a and Figure 4.17b, the shapes of the C curves are very similar to FIG. 9b) of [10], particularly in small Λ . There are also sign-alternations of C corresponding to the transformation between expansion and contraction of MTTs, which indicate the existence of TLM-DH pairs with various positive cosmological constants. By comparing with these figures, we can find that the effect of positive cosmological constant is less sensitive to the evolution parameter C in this example. The reason of this situation may be that the shrinking TLMs have already existed in this example in the absence of a cosmological constant.

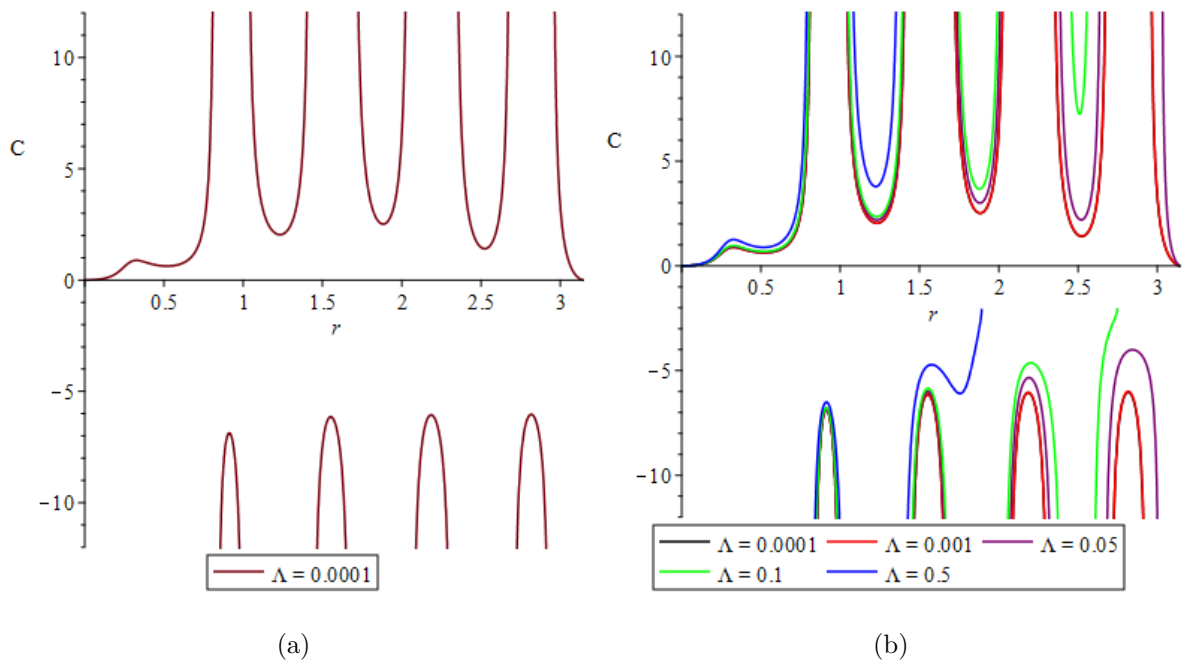


Figure 4.17: A more complicated collapse. (a) C vs r for $\Lambda = 0.0001$. (b) C vs r for various positive cosmological constants.

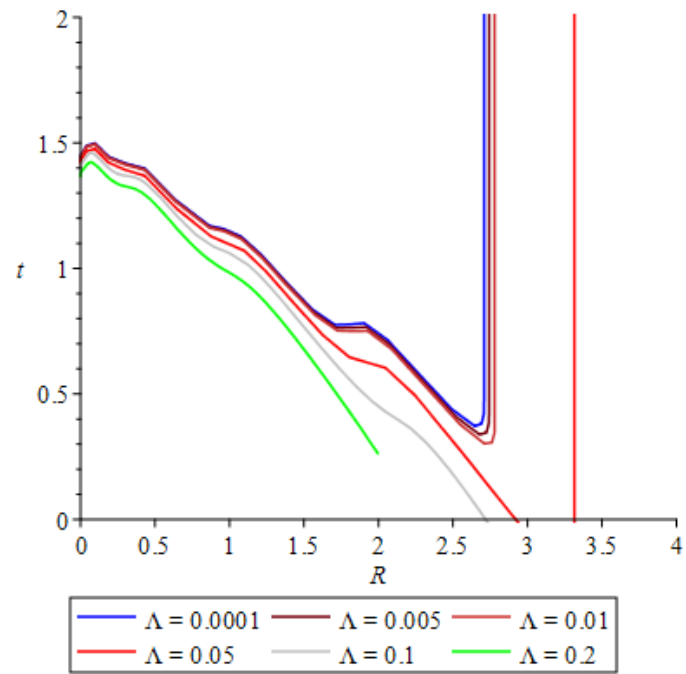


Figure 4.18: A more complicated collapse: t vs R for MTT evolution with various positive cosmological constants.

In addition, we can find that the curves of MTT evolution in Figure 4.18 have the same shape as FIG. 9c) of [10]. With the increasing positive cosmological constant, the turning point on this curve near the IH asymptote become lower until it falls below zero while the radius R of IH keeps increasing. From the curves of Figure 4.18, we can find that the model of MTT evolution for small positive Λ is the same as Section 3.5.2 of [10]¹³.

However, for large positive Λ (approximately greater than 0.05), there can be DH and TLM at the initial moment which can develop in the same mode of small positive Λ . As the previous results, when Λ is greater than the critical value (about 0.0607), there is only a shrinking TLM at the beginning of collapse¹⁴.

Besides, although the effect of positive cosmological constant Λ is relatively small in this example, we can also find that MTT evolution process is accelerated with the increasing positive Λ .

¹³In this example, the horizon firstly appear and bifurcate into DH and TLM in the outer region, and then some new horizons constantly appear and bifurcate inside the first shrinking TLM [10].

¹⁴We will discuss this situation in Chapter 5.

Chapter 5

Cosmological Horizons

As mentioned in Section 3.2, there are three solutions of Equation (3.25). The second solution R_2 , Equation (3.27b), refers to the cosmological horizon of the black hole. For an observer, the cosmological horizon (or cosmological event horizon) is the boundary of the region in which the observer can receive the signal from any points along his/her worldline [63, 64]. There can be both a black hole horizon and a cosmological horizon in black hole spacetime with positive cosmological constant Λ , while there is only a cosmological horizon in naked singularity spacetime [73].

From Equations (3.27a) and (3.27b), it is obvious that the R_1 for black hole horizon increases with the growth of positive Λ and m while the R_2 for cosmological horizon decreases. Thus, as shown in Penrose diagram of Figure 3.1, these two horizons can get close to each other with the increasing positive Λ until they coincide at $\Lambda = 1/9m^2$. The behavior of shrinking cosmological horizon can be associated with timelike membrane [10].

In this chapter, we have developed a preliminary analysis of the situations of

cosmological horizons in the formation and growing processes of black holes as the examples in Chapter 4. The physical radius R of cosmological horizon is given by Equation (3.27b). Then, we can get the evolution parameter C of cosmological horizon by Equation (3.30).

5.1 Cosmological Horizons for the Collapse of Dust Ball

In this section, we have investigated the behavior of cosmological horizons during black hole formation in the dust ball collapse. The conditions of the two examples below are the same as Section 4.1.

5.1.1 Collapse of the Dust Ball with Gaussian Initial Density

For the example of dust ball collapse with Gaussian initial mass density, we can get the curves of evolution parameter C corresponding to the cosmological horizons with various positive cosmological constants in Figure 5.1. It is not hard to find that these C curves are similar in shape to Figure 4.2 but opposite in sign. As shown in Figure 5.1b, there are also divergence of C curves with large positive Λ . However, the evolution parameter C always keeps negative in our research which means the contraction of cosmological horizon in dust ball collapse with Gaussian distribution of initial density. The shrink of cosmological horizon should accelerate first, and then slow down to stop.

Corresponding to the situation of C of cosmological horizons, Figure 5.2 shows the

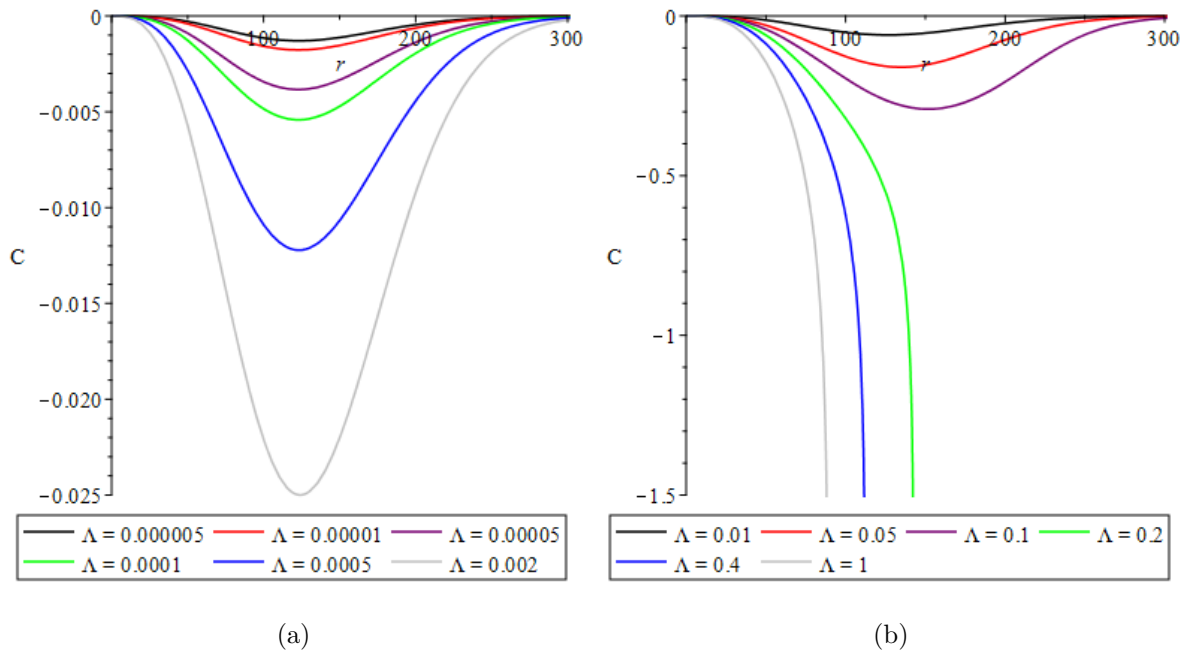


Figure 5.1: The cosmological horizons for the collapse of a dust ball. (a) C vs r for relatively small positive cosmological constants. (b) C vs r for large positive cosmological constants.

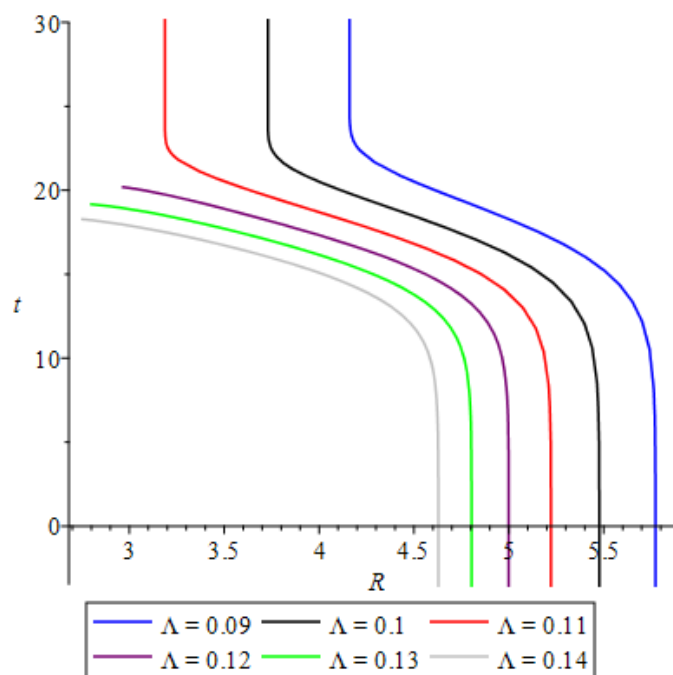


Figure 5.2: t vs R for the cosmological horizon evolution in the collapse of a dust ball with various positive cosmological constants.

evolution of cosmological horizons in the process of dust ball collapse with positive Λ . It is obvious that the shrinking cosmological horizon with relatively small positive Λ also asymptote towards a null and isolated state (like the evolution process of black hole horizon). However, for large positive Λ (greater than about 0.111), the cosmological horizon approaches the black hole horizon with the same Λ in this process which corresponds to the divergence of evolution parameter C . As shown in Figure 5.3, with the increasing positive Λ , the apparent horizon of black hole and cosmological horizon get closer and coincide with each other when $\Lambda = 1/9m^2 \approx 0.1111^1$. This behavior also correspond to the situation of the Penrose diagram in Figure 3.1. Moreover, as the situation of black hole horizon, it is not hard to find that the positive cosmological constant Λ can also accelerate the evolution process of cosmological horizon in this dust ball collapse.

5.1.2 Oppenheimer-Snyder Collapse of Inhomogeneous Dust Ball

In the example of Oppenheimer-Snyder collapse, the C curves in Figure 5.4a and 5.4b resemble the Figure 4.5a and 4.5b in shape with small σ (1/2, 1, 2) but opposite in their sign. However, for large σ (4, 8, 16), comparing with the breaking points on C curves of black hole horizons in Figure 4.5a and 4.5b, there are full curves with negative peaks for the evolution parameter C of cosmological horizons. Moreover, as shown in Figure 5.4c, for large positive Λ , there are breaking points on the curves

¹In our t vs R figures, these two horizon can be very close but there is always a small gap between them. It may be resulted from the limitation of our method.

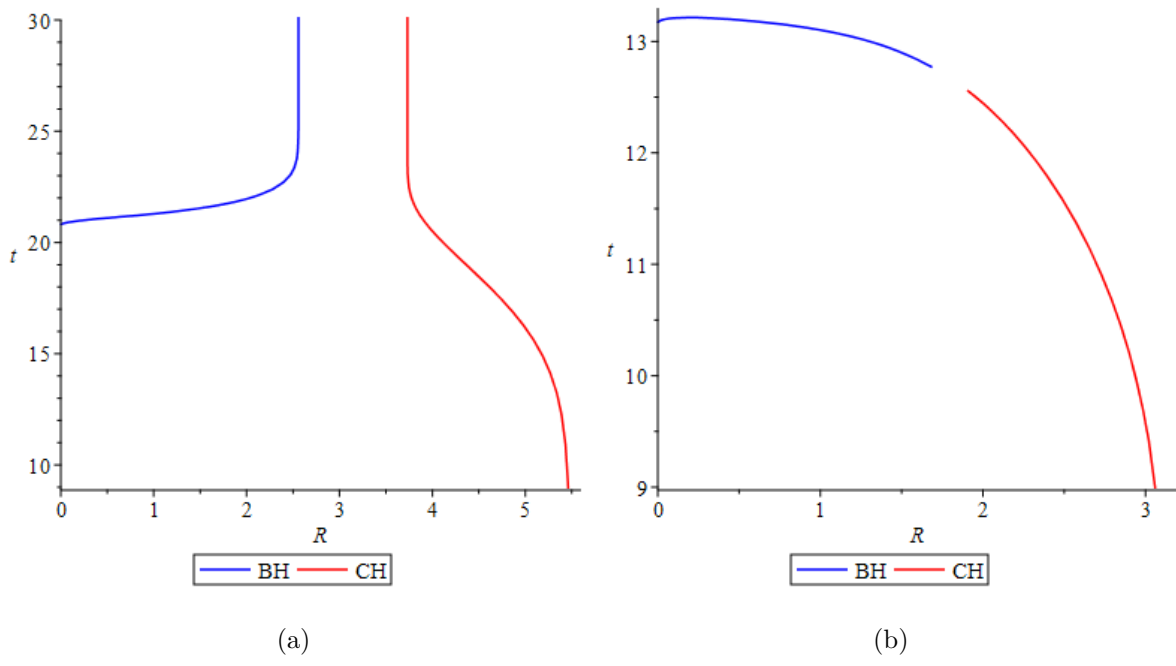


Figure 5.3: The cosmological and black hole horizons for the collapse of a dust ball.

(a) t vs R with $\Lambda = 0.1$. (b) t vs R with $\Lambda = 0.3$.

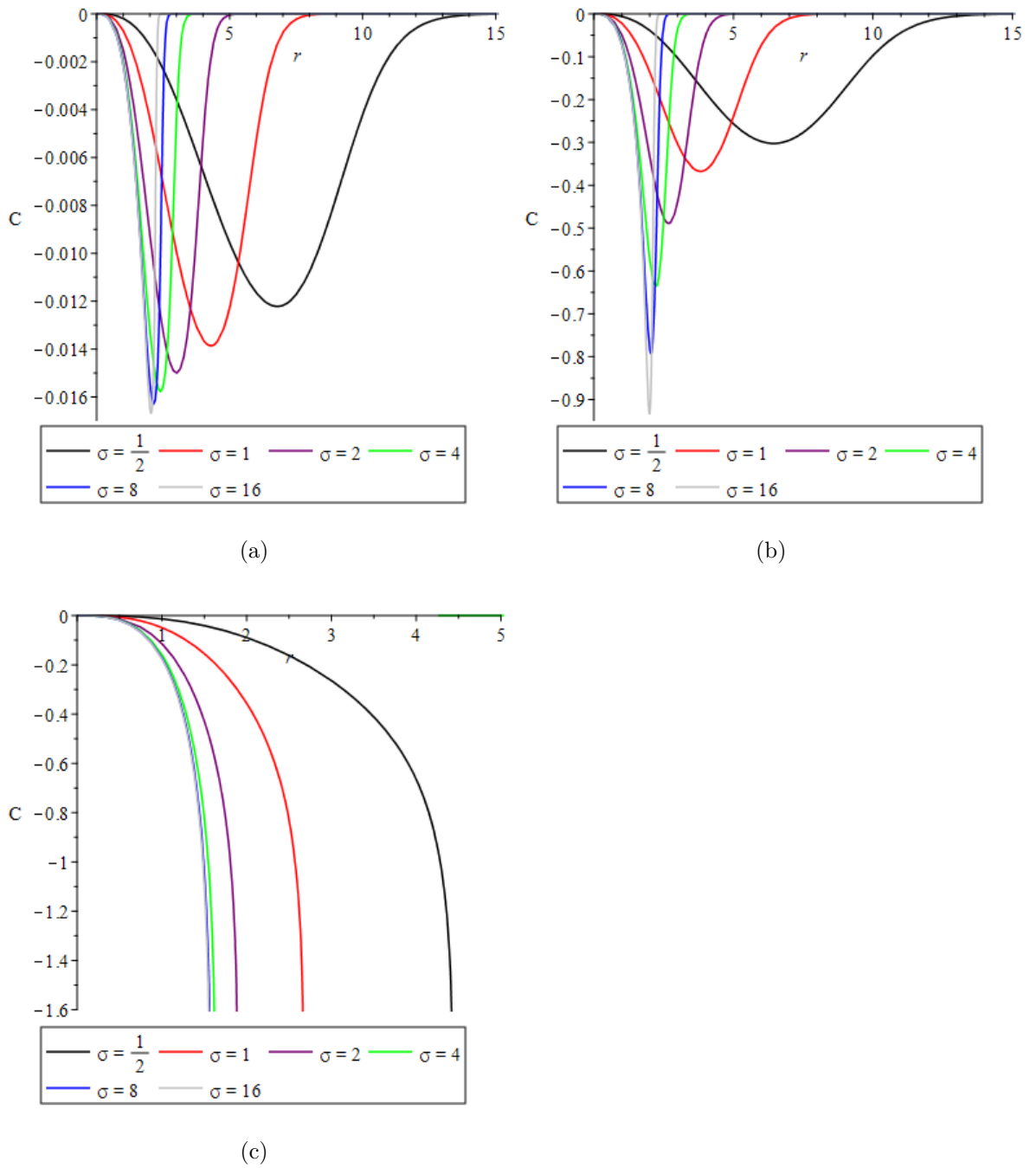


Figure 5.4: The cosmological horizons for Oppenheimer-Snyder collapse. (a) C vs r for $\Lambda = 0.0001$. (b) C vs r for $\Lambda = 0.1$. (c) C vs r for $\Lambda = 0.5$.

with all σ which refers to the situation shown in Figure 4.5c.

Similar to the situation shown in Figure 5.3, during the process of Oppenheimer-Snyder collapse, the curves in Figure 5.5 present that both the black hole and cosmological horizon can approach the null and isolated states while $\Lambda < 1/9m^2$. Obviously, with the increasing Λ , these two kinds of horizons can also get closer to each other and coincide at $\Lambda = 1/9m^2$ (approximate 0.111 in this example). Moreover, it is obvious that the processes of cosmological horizon evolution can also be accelerated in the presence of positive cosmological constants in Oppenheimer-Snyder collapse.

5.2 Cosmological Horizons for the Accretion of Dust Shells onto the Pre-existing Black Holes

In this section, we have studied the situation of cosmological horizons in the growth of black holes with dust shells infalling. The following examples are also the same as Section 4.2.

5.2.1 Small Dust Shell

As shown in Figure 5.6, for the fall of small dust shell on pre-existing black hole, the C curves of cosmological horizons are also quite similar to Figure 4.8 in shape with the opposite sign. For large positive Λ , there are also breaking points on the C curves. Hence, as the examples of dust balls, the shrinking of the cosmological horizons with relatively small positive Λ can also speed up at the beginning, and then decelerate until this process stops.

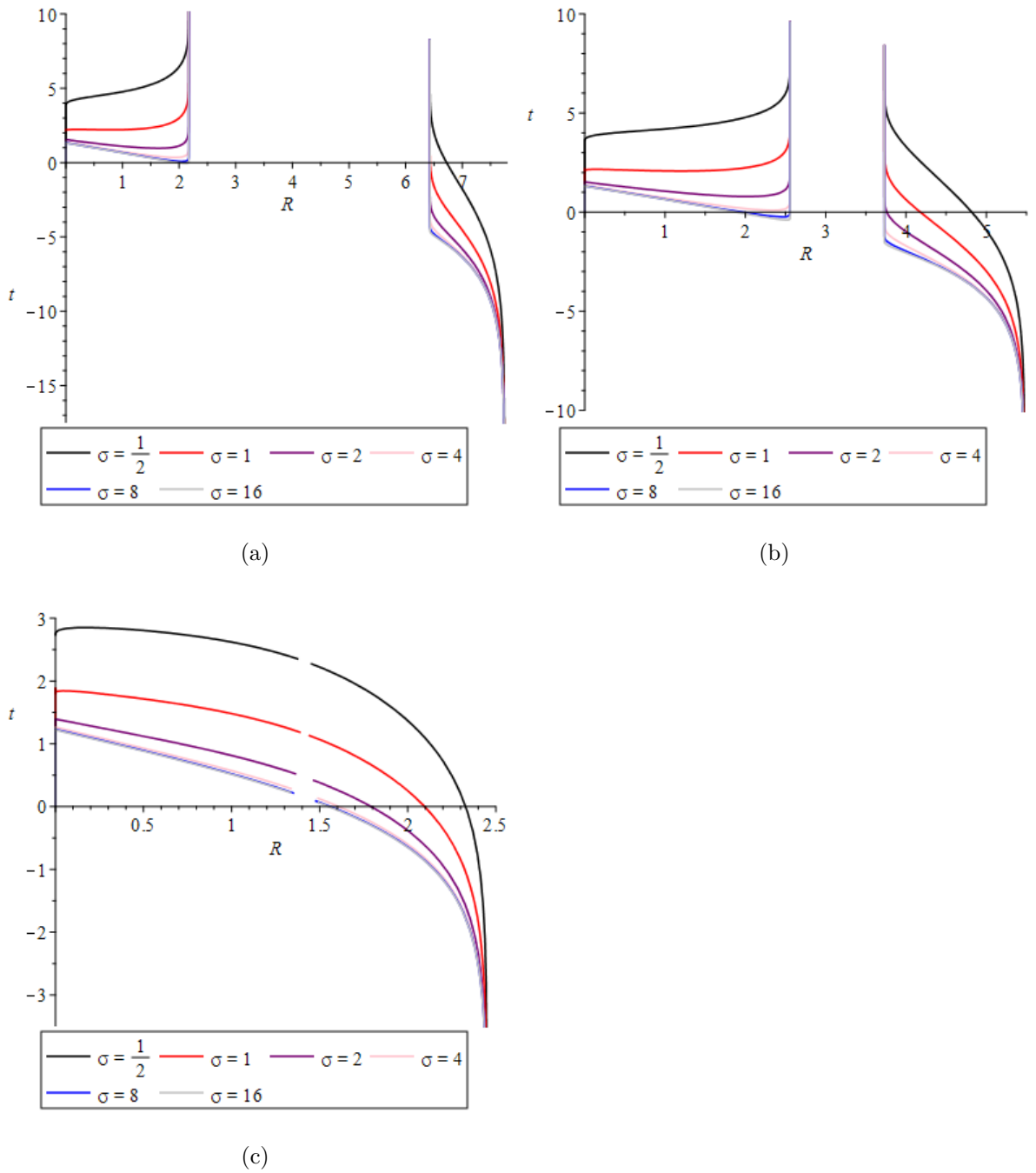


Figure 5.5: The cosmological and black hole horizons for Oppenheimer-Snyder collapse. (a) t vs R for $\Lambda = 0.05$. (b) t vs R for $\Lambda = 0.1$. (c) t vs R for $\Lambda = 0.5$

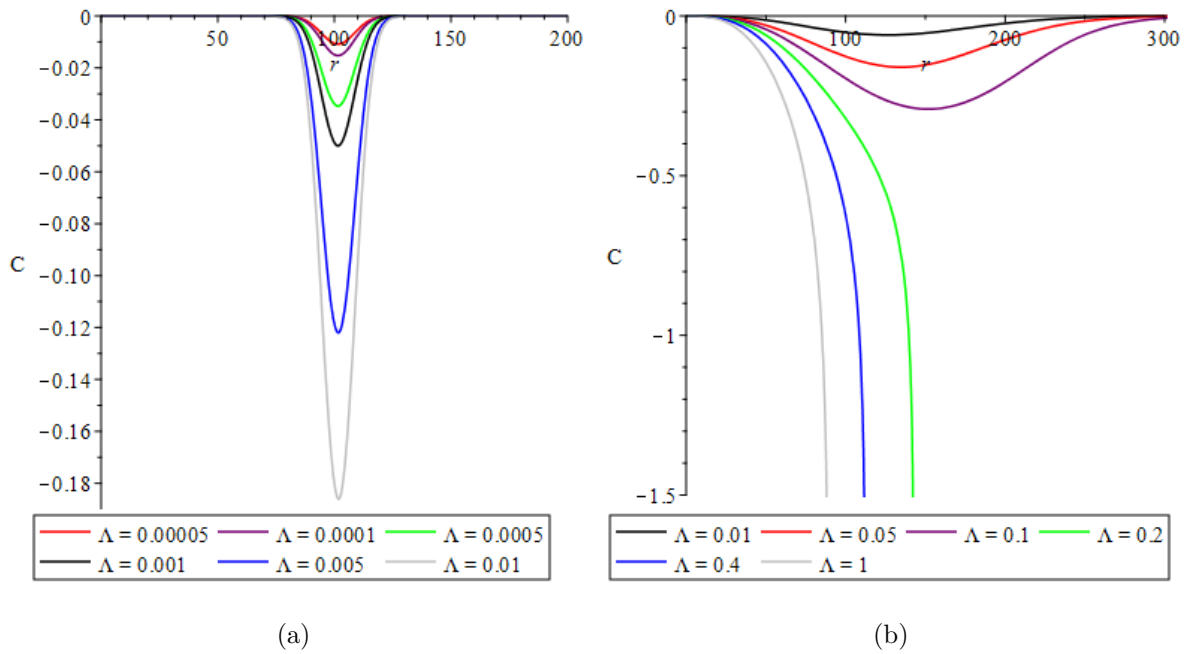


Figure 5.6: The cosmological horizons for the infalling of a small dust shell. (a) C vs r for relatively small positive cosmological constants. (b) C vs r for large positive cosmological constants.

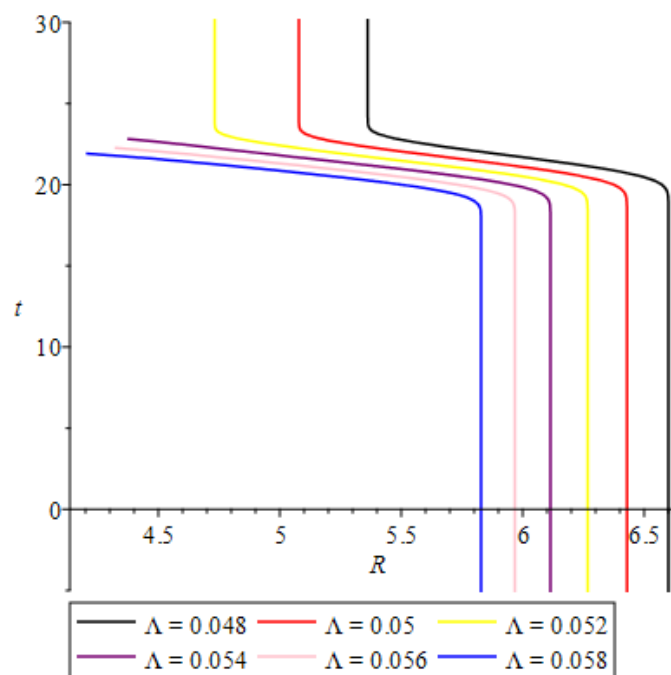


Figure 5.7: t vs R for the cosmological horizon evolution in the falling process of a small dust shell with various positive cosmological constants.

Similarly, for the evolution of the cosmological horizons in the small dust shell fall, if $\Lambda < 1/9m^2$, the R curves in Figure 5.7 would finally reach a null and isolated state too, while the curve of cosmological horizon would also approach the black hole horizon with the increasing Λ . The approaching processes between the black hole and cosmological horizons with various positive Λ are also shown in Figure 5.8. These two horizons can also coincide when Λ is greater than $1/9m^2$. Besides, it is not hard to find that the positive cosmological constant can also accelerate the evolution of cosmological horizons for the growing process of black hole in the example of small dust shell.

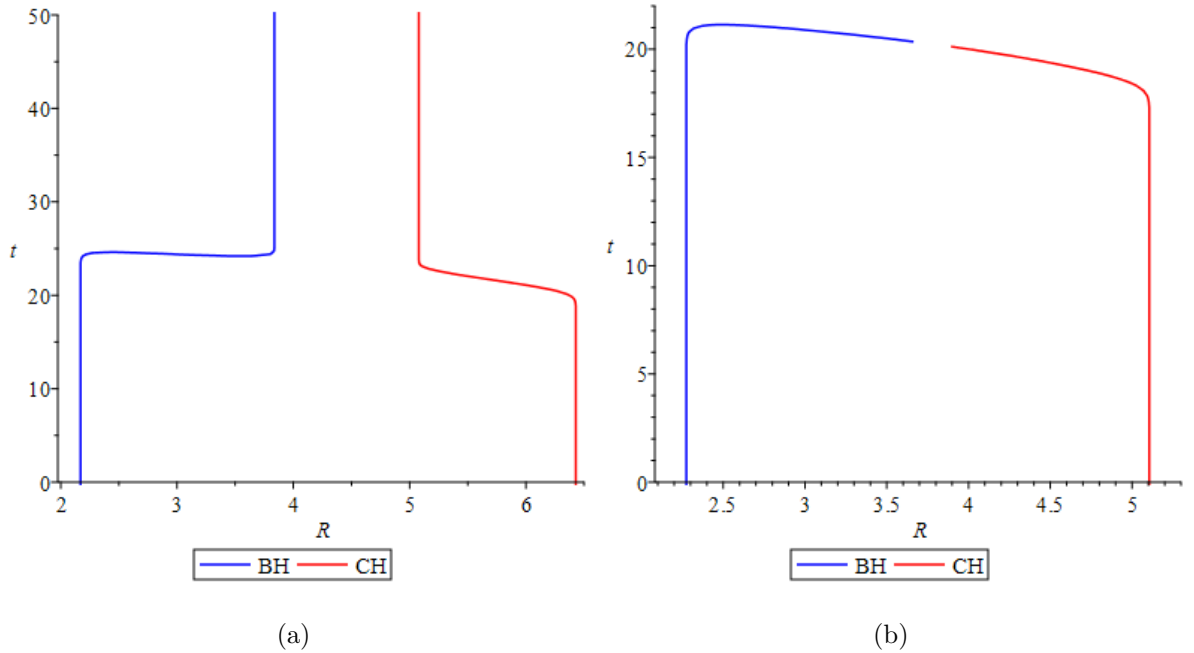


Figure 5.8: The cosmological and black hole horizons in the falling process of a dust shell. (a) t vs R with $\Lambda = 0.05$. (b) t vs R with $\Lambda = 0.07$.

5.2.2 Large Dust Shell

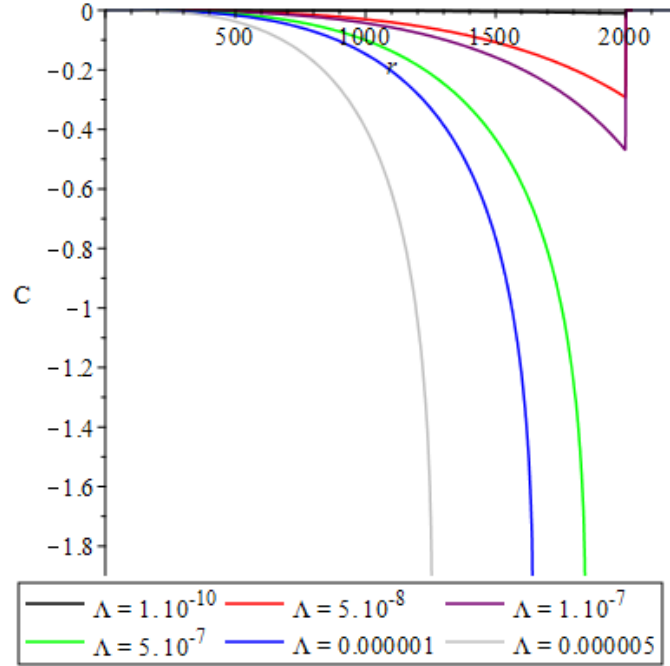


Figure 5.9: The cosmological horizons for the infalling of a large dust shell with approximately constant density: C vs r for various positive cosmological constants.

As shown in Figure 5.9, the shape of C curves is much alike to the positive part of the C curves of black hole horizons in Figure 4.11 but opposite in sign. For small positive Λ , the evolution parameter C changes from negative to zero corresponding to the process of cosmological horizons evolution (varying accelerated contraction). Moreover, there are only negative parts of the C curves with positive Λ , which means that the cosmological horizons would keep shrinking to black hole horizon. And, if Λ is greater than about 3.1×10^{-7} , the divergence of C curves would become significant greater.

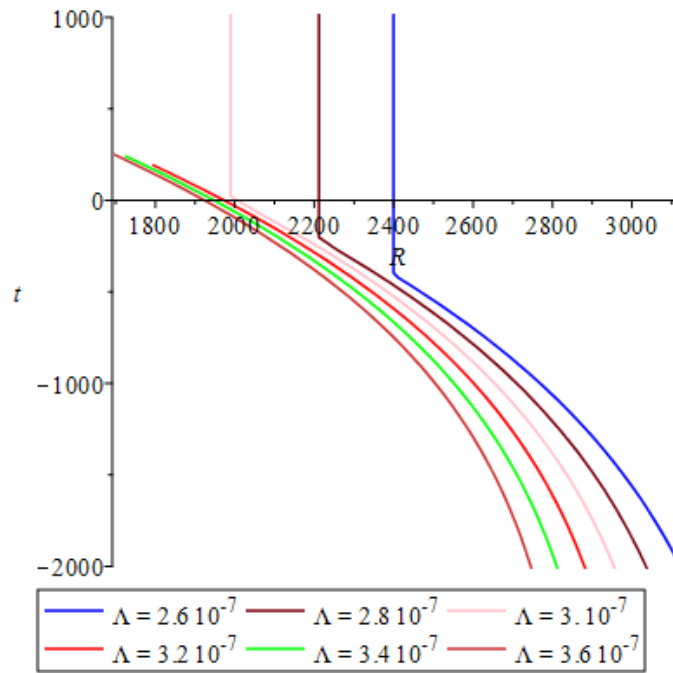


Figure 5.10: t vs R for the cosmological horizons evolution in the falling process of a large dust shell with approximately constant density for various positive cosmological constants.

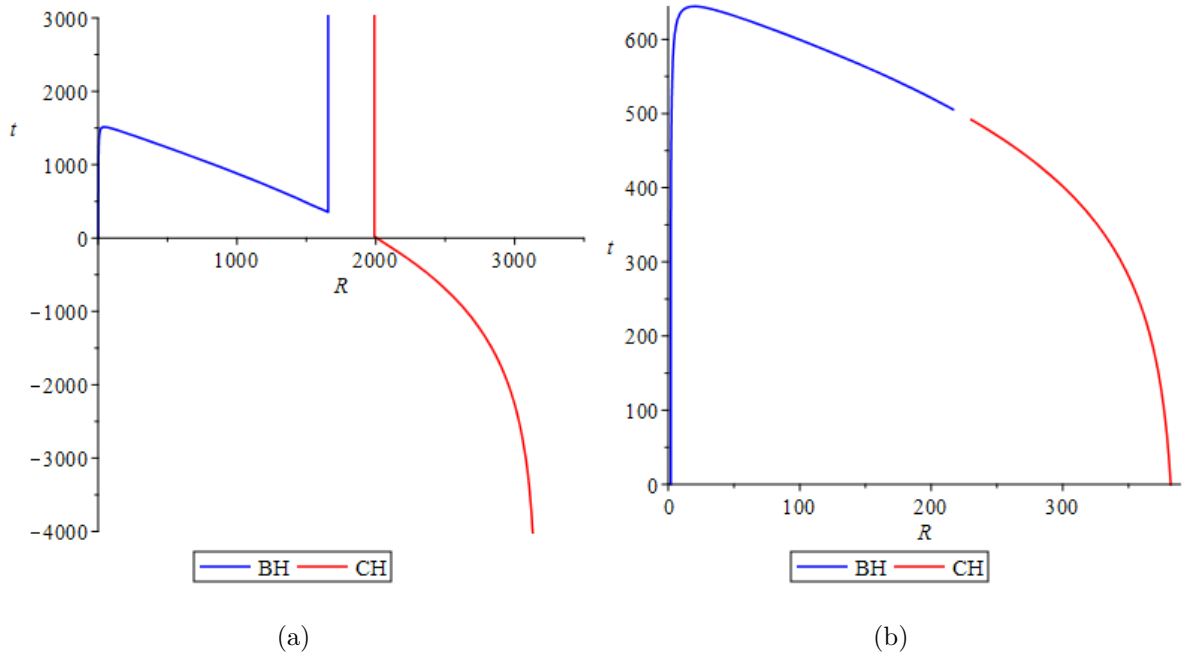


Figure 5.11: The cosmological and black hole horizons in the falling process of a large dust shell with approximately constant density. (a) t vs R with $\Lambda = 3 \times 10^{-7}$. (b) t vs R with $\Lambda = 2 \times 10^{-5}$.

As shown in Figure 5.10 ², corresponding to the behavior of evolution parameter C with various cosmological constants, the evolution curves of cosmological horizons can also approach asymptotically to a null and isolated state for relatively small positive Λ , while the evolution curves can approach the black hole horizons for large positive Λ (greater than $1/9m^2$). Meanwhile, as shown in Figure 5.11, the cosmological and black hole horizons also get closer and coincide with each other with the increasing positive Λ . Although the main parts of the curves are in the negative region of the t coordinate, we still find that the large dust shell collapse is accelerated in the presence of positive cosmological constant Λ .

5.3 Cosmological Horizons for More Complicated Collapse

In this section, we have investigated the behavior of cosmological horizons in the examples of more complicated collapse as Section 4.3.

5.3.1 Multiple Spacelike Horizons

For the example about the collapse which contains the MTT made up of multiple spacelike horizons, the behavior of corresponding cosmological horizons is shown in Figure 5.12. We can find that the evolution parameter C of the cosmological horizon also remains negative in this example. The changing of the accelerations of their

²To fully describe the processes of cosmological horizon evolution, we have to show the negative part of t coordinate.

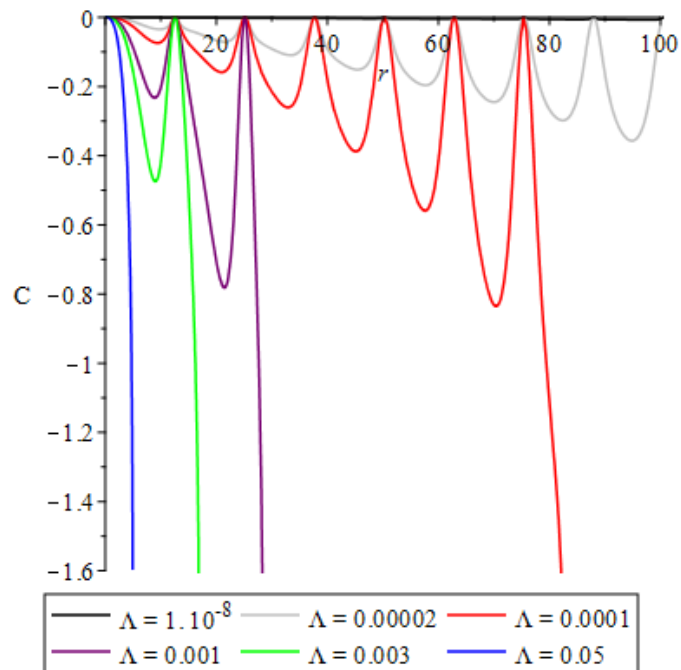


Figure 5.12: The cosmological horizons for the multiple dust shells fall into a black hole: C vs r for various positive cosmological constants.

contractions appears to be wavy which is quite similar to Figure 4.14 except for the high peaks near zero point.

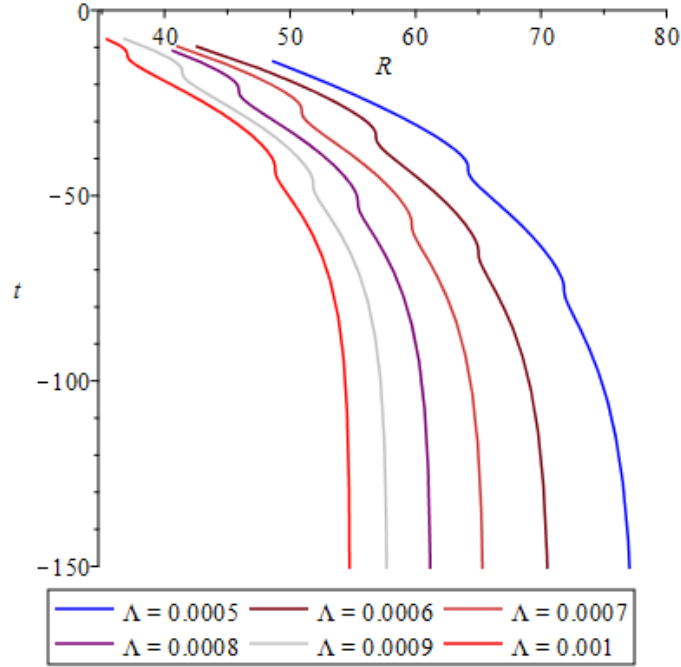


Figure 5.13: t vs R for the cosmological horizon evolution in the falling process of the multiple dust shells with various positive cosmological constants.

Moreover, as shown in Figure 5.13, the evolution curves of cosmological horizons only appear in the negative part for the t coordinate. However, from the result of Section 4.3.1, the evolution curves of black hole horizons can also extend to the negative part for the t coordinate. Hence, in Figure 5.14, the black hole and cosmological horizons can approach each other in the negative region with the increasing positive Λ . The shape of the evolution curves of cosmological horizons is also wavy which corresponds to the wavy curve of C . In addition, by comparison of the positions of the evolution curves in Figure 5.13, we can still maintain that there are accelera-

tion effects for the evolution process of the cosmological horizons with the positive cosmological constants.

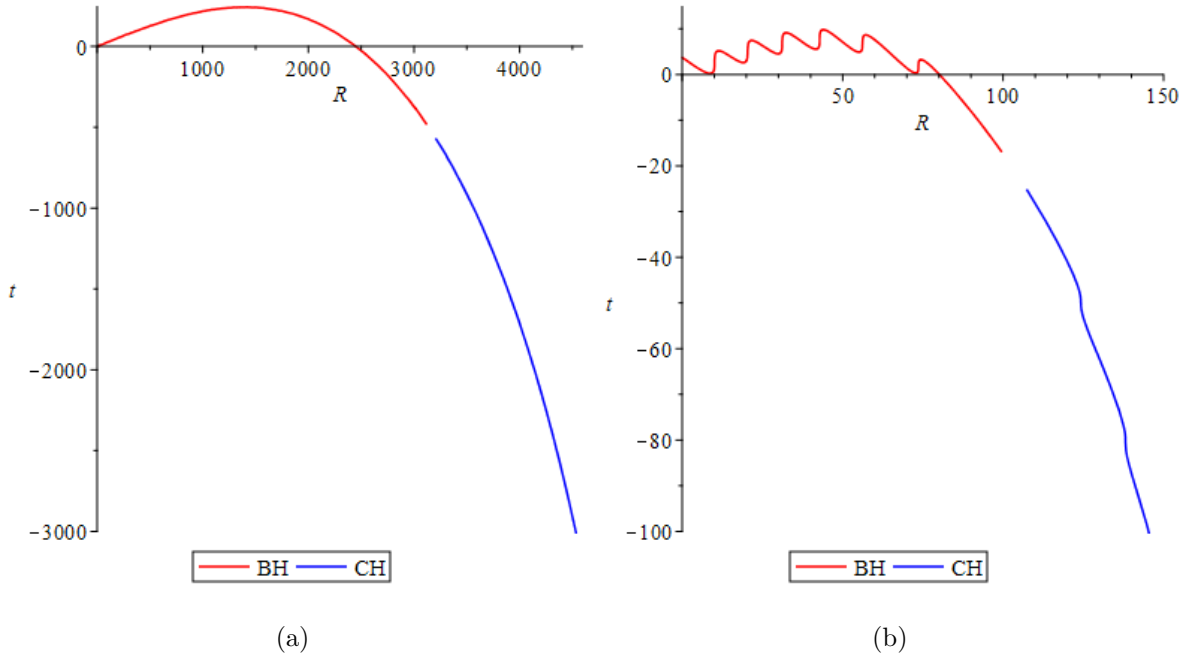


Figure 5.14: The cosmological and black hole horizons for the multiple dust shells fall into a black hole. (a) t vs R with $\Lambda = 1 \times 10^{-7}$. (b) t vs R with $\Lambda = 0.0001$.

5.3.2 Multiple Timelike Membranes

In the final example, the cosmological horizons correspond to the process of the dust collapse which contains the MTT made up of multiple dynamical horizon and timelike membrane regions. As shown in Figure 5.15, the curves of evolution parameter C for cosmological horizons with small positive cosmological constant Λ change from negative to zero between $r = 0$ and π , while the C curves with large positive Λ

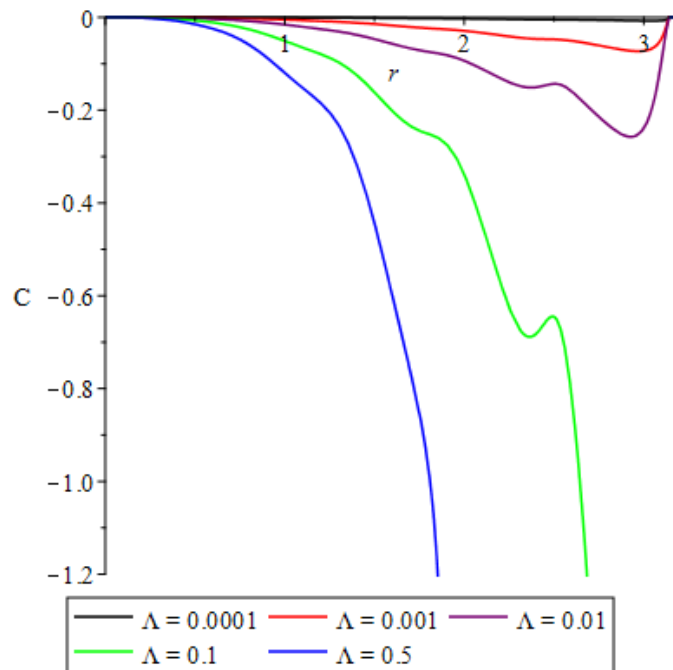


Figure 5.15: The cosmological horizons for a more complicated collapse: C vs r for various positive cosmological constants.

(greater than approximate 0.0606) is divergent near $r = \pi$.

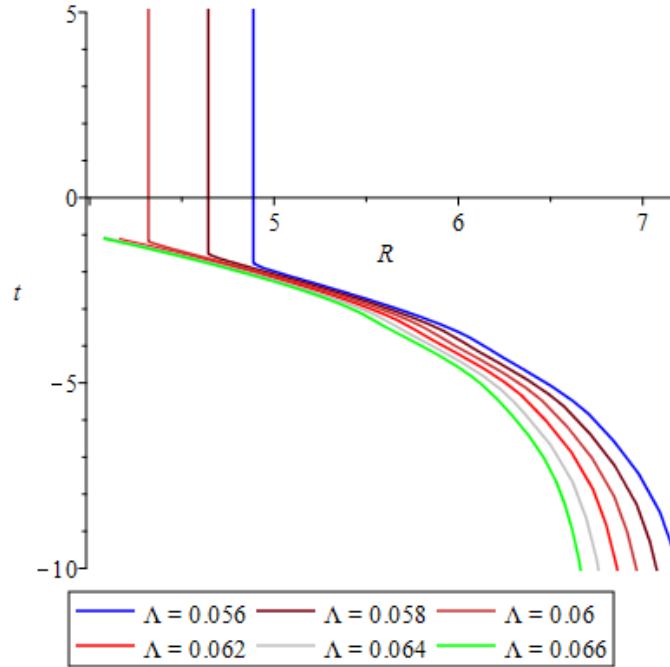


Figure 5.16: t vs R for the cosmological horizon evolution in a more complicated dust collapse with various positive cosmological constants.

The curves of cosmological horizon evolution in Figure 5.16 are mainly located in the region of the negative t coordinate, the shapes of these curves refer to the result of Figure 5.15. The curves with relatively small positive Λ can also asymptote towards a null and isolated state over time, while they can approach the black hole horizons with large positive Λ (greater than 0.0606). Similar to the previous examples, as shown in Figure 5.17, the cosmological and black hole horizons can also get closer and coincide with the increasing positive Λ . Furthermore, the cosmological horizon evolution is also accelerated in the presence of positive Λ .

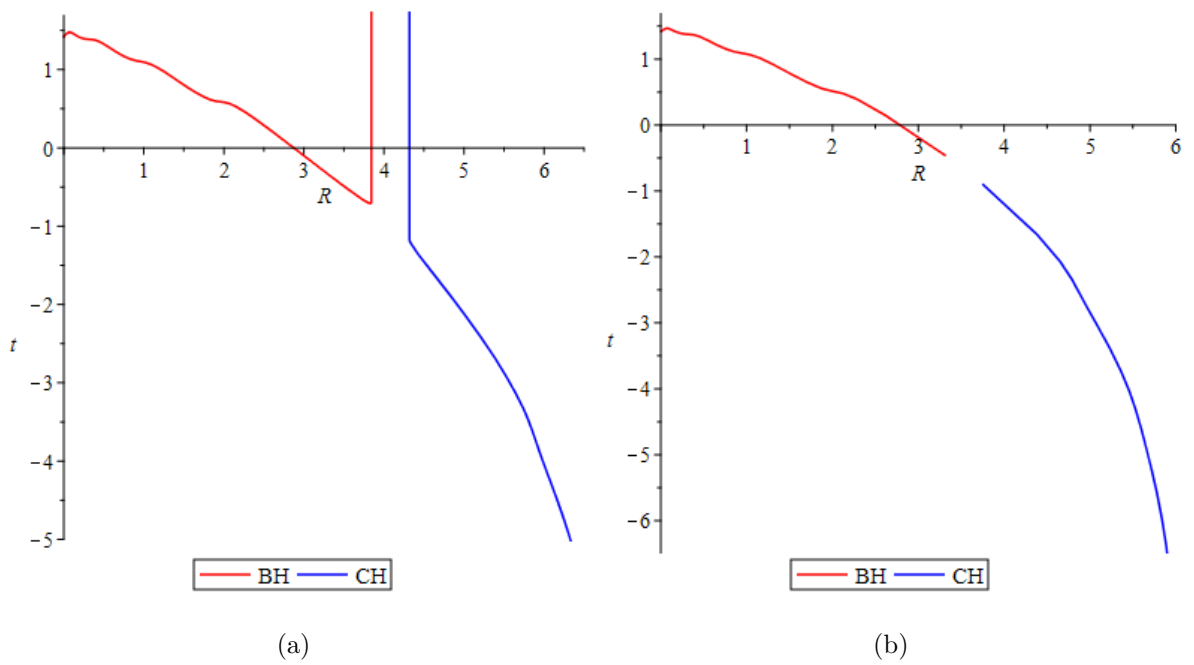


Figure 5.17: The cosmological and black hole horizons for a more complicated dust collapse. (a) t vs R with $\Lambda = 0.06$. (b) t vs R with $\Lambda = 0.08$.

Chapter 6

Conclusions and Future Studies

In this final chapter, we summarise the results of this thesis and point out some prospective studies. In this thesis, we investigated the behaviors of black hole boundaries in the presence of positive cosmological constant Λ . We have found that the effects of positive Λ are quite obvious on the formation and growth of black holes in some examples of dust cloud collapse.

6.1 Conclusions and Discussions

In the first chapter, the background knowledge and motivation of this thesis were introduced briefly. Black hole is considered as the most successful application of general relativity, and the study of cosmological constant Λ is a significant part of modern physics. In Chapter 2, we presented brief definitions of standard and quasilocal horizons of black holes. In this thesis, we have focused on the quasilocal horizons of black holes. Chapter 3 mainly introduced the properties of spherically symmetric MTT and some relative research methods in the presence of positive cosmological constant

Λ . We investigated the behavior of MTT evolution during the formation and growth of black hole in the spherically symmetric dust cloud collapse in TBdS spacetime theoretically. In Chapter 4, we applied the obtained results to six examples about spherical dust clouds collapse with different initial mass densities and positive cosmological constants. By comparing the results of Chapter 4 with [10], we have found that the positive cosmological constant Λ indeed has significant effects on the behavior of MTT evolution during the processes of black hole formation and development in gravitational collapse of dust clouds, particularly for large positive Λ . Moreover, in Chapter 5, we made some preliminary investigation of the behavior of cosmological horizons in the same examples of dust cloud collapse in the presence of positive Λ . We have found that the cosmological horizons are associated with the black hole horizons.

The results of Chapter 4 have shown that the evolution of MTTs can be obviously influenced by the values of positive cosmological constant Λ . By comparing with the zero cosmological constant case in [10], the curves of the evolution parameter C for relatively small Λ can still preserve their shape with similarity to the results of [10]. The small Λ can increase the values of parameter C , which have indicated the accelerated effect of positive cosmological constant Λ for the horizon evolution. Besides, while the positive cosmological constant Λ is greater than some critical values¹, there are significant shape variations for C curves which indicate the appearance and evolution of new horizon (such as timelike membrane) during the concentrations of dust clouds in our examples (except for Section 4.3.1). This behavior of MTT evolu-

¹The critical value of Λ may be determined by $1/(9m^2)$. In these examples, the critical values usually differ by orders of magnitude due to the various mass densities of the dust clouds.

tion primarily matches the prediction about the appearance of TLM in formation or growth of black hole in the presence of a cosmological constant given by Dr. Booth in [10].

Moreover, in some examples (such as Section 4.1.1, 4.2.1, and 4.3.1) under the condition of large positive cosmological constant, the new horizons may appear in the regions outside the original horizons². Furthermore, some new horizons may bifurcate into the pairs of expanding DHs and contracting TLMs immediately, while these DHs and TLMs would merge with each other or vanish into singularities over time. Besides, by analysis of the variation of MTT evolution with positive Λ , it is not hard for us to find the accelerated effect of positive cosmological constant on the process of MTT evolution in dust cloud collapse. The main reason of this acceleration may be that the positive Λ has the same effect on the concentrations of dust clouds as a kind of extra pressure from outside³.

For the second solution of Equation (3.25), there are corresponding cosmological horizon in the formation and growing processes of black holes. In Chapter 5, the behavior of cosmological horizons associated with the black hole horizons in the same examples of dust clouds collapse was primarily studied. The evolution parameter C for cosmological horizon remains negative corresponding to the contraction of these horizons. With the increasing positive cosmological constant Λ , the shrinking cosmological horizons would approach the black hole horizons and finally coincide with them⁴ (when $\Lambda \geq 1/(9m^2)$). Similar to the black hole horizons, the evolution of

²This phenomenon may be related to “horizon jumps” [10, 40].

³Typically, positive cosmological constant causes the expansion in a spacetime, so the collapse process was expected to be slower in the presence of positive Λ .

⁴In our results, there are always small gaps between cosmological and black hole horizons due to

cosmological horizons can also be accelerated with the increasing positive Λ .

6.2 Future Studies

In this thesis, we have found that the behavior of marginally trapped tubes during black hole evolution is obviously influenced by the presence of positive cosmological constant. In fact, the model and examples used in our research are quite simplified. In this thesis, the definition of the mass of dust system did not include the effect of the positive cosmological constant Λ . Thus, our results are not perfect, especially for the examples under more complicated conditions. Hence, in prospective investigation following this study, we plan to introduce the Λ term in the mass density of dust cloud and research the impact of this variation on the MTT evolution during the formation or growth of black hole in the dust cloud collapse. Furthermore, the conditions of this study are electric neutral and non-rotating, so we may add some affecting factors in our future work, such as electric charge Q , angular momentum J , and magnetic field \mathcal{M} ⁵ (like Kerr-Newman black hole in Appendix A.2.2).

Moreover, in Chapter 5, we just made preliminary investigation on the behaviors of cosmological horizons in those examples. So there are still many issues that require further study and discussion. We can research the evolution process of the cosmological horizon with negative C in dust cloud collapse in more detail, particularly for coincidence with black hole horizons.

In addition, we can also extend our future research on other problems in cosmology.

the limitation of our method

⁵The magnetic field \mathcal{M} may be generated by electric charge Q and rotation.

The values of cosmological constant used in this thesis are all quite large which may be related to the situation of quantum field theory or the early universe [67, 75, 81]. Thus, it may be possible to make a research on the cosmological constant problem from the aspect about the evolution of black hole horizons.

Bibliography

- [1] T. Adamo and E. Newman. The Kerr-Newman metric: a review. *arXiv preprint arXiv:1410.6626*, 2014.
- [2] S. Akcay and R. A. Matzner. The Kerr–de Sitter universe. *Classical and Quantum Gravity*, 28(8):085012, 2011.
- [3] L. Andersson, M. Mars, and W. Simon. Stability of marginally outer trapped surfaces and existence of marginally outer trapped tubes. *arXiv preprint arXiv:0704.2889*, 2007.
- [4] A. Ashtekar, C. Beetle, O. Dreyer, S. Fairhurst, B. Krishnan, J. Lewandowski, and J. Wiśniewski. Generic isolated horizons and their applications. *Physical Review Letters*, 85(17):3564, 2000.
- [5] A. Ashtekar, G. J. Galloway, et al. Some uniqueness results for dynamical horizons. *Advances in Theoretical and Mathematical Physics*, 9(1):1–30, 2005.
- [6] A. Ashtekar and B. Krishnan. Isolated and dynamical horizons and their applications. *Living Reviews in Relativity*, 7(1):10, 2004.

- [7] V. Balasubramanian, J. De Boer, and D. Minic. Mass, entropy, and holography in asymptotically de Sitter spaces. *Physical Review D*, 65(12):123508, 2002.
- [8] I. Bengtsson, E. Jakobsson, and J. M. Senovilla. Trapped surfaces in Oppenheimer-Snyder black holes. *Physical Review D*, 88(6):064012, 2013.
- [9] I. Booth. Black-hole boundaries. *Canadian journal of physics*, 83(11):1073–1099, 2005.
- [10] I. Booth, L. Brits, J. A. Gonzalez, and C. Van Den Broeck. Marginally trapped tubes and dynamical horizons. *Classical and Quantum Gravity*, 23(2):413, 2005.
- [11] I. Booth and S. Fairhurst. Isolated, slowly evolving, and dynamical trapping horizons: Geometry and mechanics from surface deformations. *Physical Review D*, 75(8):084019, 2007.
- [12] I. S. Booth. A quasilocal Hamiltonian for gravity with classical and quantum applications. *arXiv preprint gr-qc/0008030*, 2000.
- [13] R. Bousso. Adventures in de Sitter space. *arXiv preprint hep-th/0205177*, 2002.
- [14] R. Bousso and S. W. Hawking. (Anti-) evaporation of Schwarzschild–de Sitter black holes. *Physical Review D*, 57(4):2436, 1998.
- [15] L. Canbin and Z. Bin. *Introduction to Differential Geometry and General Relativity*. China Science Publishing and Media Ltd, 2009.
- [16] V. Cardoso and J. P. Lemos. Quasinormal modes of the near extremal Schwarzschild–de Sitter black hole. *Physical Review D*, 67(8):084020, 2003.

- [17] S. M. Carroll. The cosmological constant. *Living reviews in relativity*, 4(1):1, 2001.
- [18] S. M. Carroll. *Spacetime and geometry. An introduction to general relativity*. 2004.
- [19] R. Casadio and B. Harms. Microcanonical description of (micro) black holes. *Entropy*, 13(2):502–517, 2011.
- [20] R. Casadio and P. Nicolini. The decay-time of non-commutative micro-black holes. *Journal of High Energy Physics*, 2008(11):072, 2008.
- [21] J. Casares. Observational evidence for stellar-mass black holes. *Proceedings of the International Astronomical Union*, 2(S238):3–12, 2006.
- [22] A. Celotti, J. Miller, and D. Sciama. Astrophysical evidence for the existence of black holes. *Classical and Quantum Gravity*, 16:A3, 1999.
- [23] S. Chakraborty, S. Bhattacharya, and T. Padmanabhan. Entropy of a generic null surface from its associated Virasoro algebra. *Physics Letters B*, 763:347–351, 2016.
- [24] T. E. H. T. Collaboration. First M87 Event Horizon Telescope Results. I. The Shadow of the Supermassive Black Hole. *The Astrophysical Journal Letter*, 875(1), 2019.
- [25] B. P. Dolan. The cosmological constant and black-hole thermodynamic potentials. *Classical and Quantum Gravity*, 28(12):125020, 2011.

- [26] K. Duggal. Foliations of lightlike hypersurfaces and their physical interpretation. *Open Mathematics*, 10(5):1789–1800, 2012.
- [27] V. Faraoni. *Cosmological and black hole apparent horizons*. Springer, 2015.
- [28] A. Franzen, S. Gutti, and C. Kiefer. Quantum gravitational collapse in the Lemaitre-Tolman-Bondi model with a positive cosmological constant. *Classical and Quantum Gravity*, 27(1):015011, 2009.
- [29] V. Frolov and I. Novikov. *Black hole physics: basic concepts and new developments*, volume 96. Springer Science & Business Media, 2012.
- [30] V. P. Frolov and A. Zelnikov. *Introduction to black hole physics*. OUP Oxford, 2011.
- [31] S. Funkhouser. A fundamental scale of mass for black holes from the cosmological constant. *arXiv preprint physics/0701289*, 2007.
- [32] A. Ghez, S. Salim, N. Weinberg, J. Lu, T. Do, J. Dunn, K. Matthews, M. Morris, S. Yelda, E. Becklin, et al. Measuring distance and properties of the Milky Way’s central supermassive black hole with stellar orbits. *The Astrophysical Journal*, 689(2):1044, 2008.
- [33] S. M. Gonçalves. Naked singularities in Tolman–Bondi–de Sitter collapse. *Physical Review D*, 63(6):064017, 2001.
- [34] S. M. Gonçalves. Shell crossing in generalized Tolman-Bondi spacetimes. *Physical Review D*, 63(12):124017, 2001.

- [35] S. M. Gonçalves. Strength and genericity of singularities in Tolman–Bondi–de Sitter collapse. *Physics Letters A*, 287(1-2):53–58, 2001.
- [36] B. Grado-White and D. Marolf. Marginally trapped surfaces and AdS/CFT. *Journal of High Energy Physics*, 2018(2):49, 2018.
- [37] A. W. Graham and N. Scott. The (Black Hole)-bulge Mass Scaling Relation at Low Masses. *The Astrophysical Journal*, 798(1), 2015.
- [38] J. Hajj-Boutros. Spherically symmetric perfect fluid solutions in isotropic coordinates. *Journal of mathematical physics*, 27(5):1363–1366, 1986.
- [39] J. Hartle. *Gravity: An Introduction to Einstein’s General Relativity*. Addison Wesley, 2003.
- [40] S. W. Hawking and G. F. R. Ellis. *The large scale structure of space-time*, volume 1. Cambridge university press, 1973.
- [41] S. A. Hayward. General laws of black-hole dynamics. *Physical Review D*, 49(12):6467, 1994.
- [42] S. A. Hayward. Black holes: New horizons. *arXiv preprint gr-qc/0008071*, 2000.
- [43] C. Hellaby. On the Vaidya limit of the Tolman model. *Physical Review D*, 49(12):6484, 1994.
- [44] A. Helou. Dynamics of the four kinds of Trapping Horizons and Existence of Hawking Radiation. *arXiv preprint arXiv:1505.07371*, 2015.

- [45] J. Hlavacek-Larrondo, A. Fabian, A. Edge, and M. Hogan. On the hunt for ultramassive black holes in brightest cluster galaxies. *Monthly Notices of the Royal Astronomical Society*, 424(1):224–231, 2012.
- [46] S. A. Hughes. Trust but verify: The case for astrophysical black holes. *arXiv preprint hep-ph/0511217*, 2005.
- [47] K. Jedamzik and J. C. Niemeyer. Primordial black hole formation during first-order phase transitions. *Physical Review D*, 59(12):124014, 1999.
- [48] R. Konoplich, S. Rubin, A. Sakharov, and M. Y. Khlopov. Formation of black holes in first-order phase transitions in the universe. *Astronomy Letters*, 24:413–417, 1998.
- [49] B. Krishnan. Quasi-local black hole horizons. In *Springer Handbook of Spacetime*, pages 527–555. Springer, 2014.
- [50] L. Liu and Z. Zhao. *General Relativity*. Higher Education Press, 2006.
- [51] L. Liu, Z. Zhao, G. Tian, and J. Zhang. *Properties of Black Hole and Time*. Peking University Press, 2008.
- [52] Y. Liu and S. N. Zhang. Exact solutions for shells collapsing towards a pre-existing black hole. *Physics Letters B*, 679(2):88–94, 2009.
- [53] D. Markovic and S. L. Shapiro. Gravitational collapse with a cosmological constant. *Physical Review D*, 61(8):084029, 2000.
- [54] P. Natarajan and E. Treister. Is there an upper limit to black hole masses? *Monthly Notices of the Royal Astronomical Society*, 393(3):838–845, 2009.

- [55] J. R. Oppenheimer and G. M. Volkoff. On massive neutron cores. *Physical Review*, 55(4):374, 1939.
- [56] A. Ori. The general solution for spherical charged dust. *Classical and Quantum Gravity*, 7(6):985, 1990.
- [57] A. Padilla. Lectures on the cosmological constant problem. *arXiv preprint arXiv:1502.05296*, 2015.
- [58] T. Padmanabhan and A. Paranjape. Entropy of null surfaces and dynamics of spacetime. *Physical Review D*, 75(6):064004, 2007.
- [59] R. Penrose. Gravitational collapse and space-time singularities. *Physical Review Letters*, 14(3):57, 1965.
- [60] J. Plebanski and A. Krasinski. *An introduction to general relativity and cosmology*. Cambridge University Press, 2006.
- [61] E. Poisson. *A relativist's toolkit: the mathematics of black-hole mechanics*. Cambridge university press, 2004.
- [62] E. Polášková and O. Svítek. Quasilocal horizons in inhomogeneous cosmological models. *Classical and Quantum Gravity*, 36(2):025005, 2018.
- [63] H. S. Reall. Lecture Notes: Part 3 Black holes. http://www.damtp.cam.ac.uk/user/hsr1000/black_holes_lectures_2016.pdf, 2008.
- [64] H. S. Reall. Lecture Notes: Part 3 General Relativity. http://www.damtp.cam.ac.uk/user/hsr1000/part3_gr_lectures_2017.pdf, 2013.

- [65] V. A. Rubakov. The null energy condition and its violation. *Physics-Uspexhi*, 57(2):128, 2014.
- [66] S. E. Rugh and H. Zinkernagel. The quantum vacuum and the cosmological constant problem. *Studies In History and Philosophy of Science Part B: Studies In History and Philosophy of Modern Physics*, 33(4):663–705, 2002.
- [67] V. Sahni. The cosmological constant problem and quintessence. *Classical and Quantum Gravity*, 19(13):3435, 2002.
- [68] E. Schnetter, B. Krishnan, and F. Beyer. Introduction to dynamical horizons in numerical relativity. *Physical Review D*, 74(2):024028, 2006.
- [69] S. Shankaranarayanan. Temperature and entropy of Schwarzschild–de Sitter space-time. *Physical Review D*, 67(8):084026, 2003.
- [70] S. L. Shapiro and S. A. Teukolsky. *Black Holes, White Dwarfs and Neutron Star: The Physics of Compact objects*. WILEY-VCH Verlag GmbH and Co. KgaA, 2004.
- [71] N. Straumann. On the cosmological constant problems and the astronomical evidence for a homogeneous energy density with negative pressure. In *Poincaré Seminar 2002*, pages 7–51. Springer, 2003.
- [72] Z. Stuchlík and S. Hledík. Some properties of the Schwarzschild–de Sitter and Schwarzschild–anti-de Sitter spacetimes. *Physical Review D*, 60(4):044006, 1999.
- [73] Z. Stuchlík and P. Slaný. Equatorial circular orbits in the Kerr–de Sitter spacetimes. *Physical Review D*, 69(6):064001, 2004.

- [74] R. A. Sussman and G. Izquierdo. A dynamical system study of the inhomogeneous Λ -CDM model. *Classical and Quantum Gravity*, 28(4):045006, 2011.
- [75] A. Tawfik. The Hubble parameter in the early universe with viscous QCD matter and finite cosmological constant. *Annalen der Physik*, 523(5):423–434, 2011.
- [76] J. Thornburg. Event and apparent horizon finders for 3+ 1 numerical relativity. *Living reviews in relativity*, 10(1):3, 2007.
- [77] N. Tomohiro and Y. Jun'ichi. Micro black holes formed in the early Universe and their cosmological implications. *Phys. Rev. D*, 99:061303, 2019.
- [78] M. Visser. The Kerr spacetime: A brief introduction. *arXiv preprint arXiv:0706.0622*, 2007.
- [79] M. Visser. Physical observability of horizons. *Physical Review D*, 90(12):127502, 2014.
- [80] R. M. Wald. General relativity(Book). *Chicago, University of Chicago Press, 1984, 504 p*, 1984.
- [81] S. Weinberg. The cosmological constant problem. *Reviews of modern physics*, 61(1):1, 1989.
- [82] C. Williams. A black hole with no marginally trapped tube asymptotic to its event horizon. *Complex Analysis and Dynamical Systems IV: General relativity, geometry, and PDE*, 2:253, 2011.
- [83] S. Xiang. *Introduction to Astrophysics*. USTC Press, 2008.

- [84] W. Yongjiu. *Gravitational Theory*. China Science Publishing and Media Ltd, 2011.
- [85] I. Zehavi and A. Dekel. Evidence for a positive cosmological constant from flows of galaxies and distant supernovae. *Nature*, 401(6750):252, 1999.

Appendix A

Classification of Black Holes

A.1 The Size of Black Holes

In astrophysics, the black holes can be classified into four major types by size:

1. **Micro black hole** (quantum mechanical black hole or mini black hole) is a kind of hypothetical tiny black hole which may exist in microscopic scale. The mass of micro black hole may be just a few TeV's¹ [19, 20]. Quantum effect plays an important role in them. Micro black hole may form at the high temperature and high density rather than by the gravitational collapse of a stellar (primordial black hole may form during first-order phase transitions in early universe after the big bang) [22, 47, 48, 77].

2. **Stellar black hole** is produced by the gravitational collapse of a massive star with mass typically in the range of $5M_{\odot}$ to $100M_{\odot}$ ² [46]. We may find stellar

¹ $1 \text{ TeV}/c^2 \approx 1.78266 \times 10^{-24} \text{ Kg}$.

² The stellar mass must exceed the Tolman-Oppenheimer-Volkoff limit (about $2.9M_{\odot}$) [21, 55].

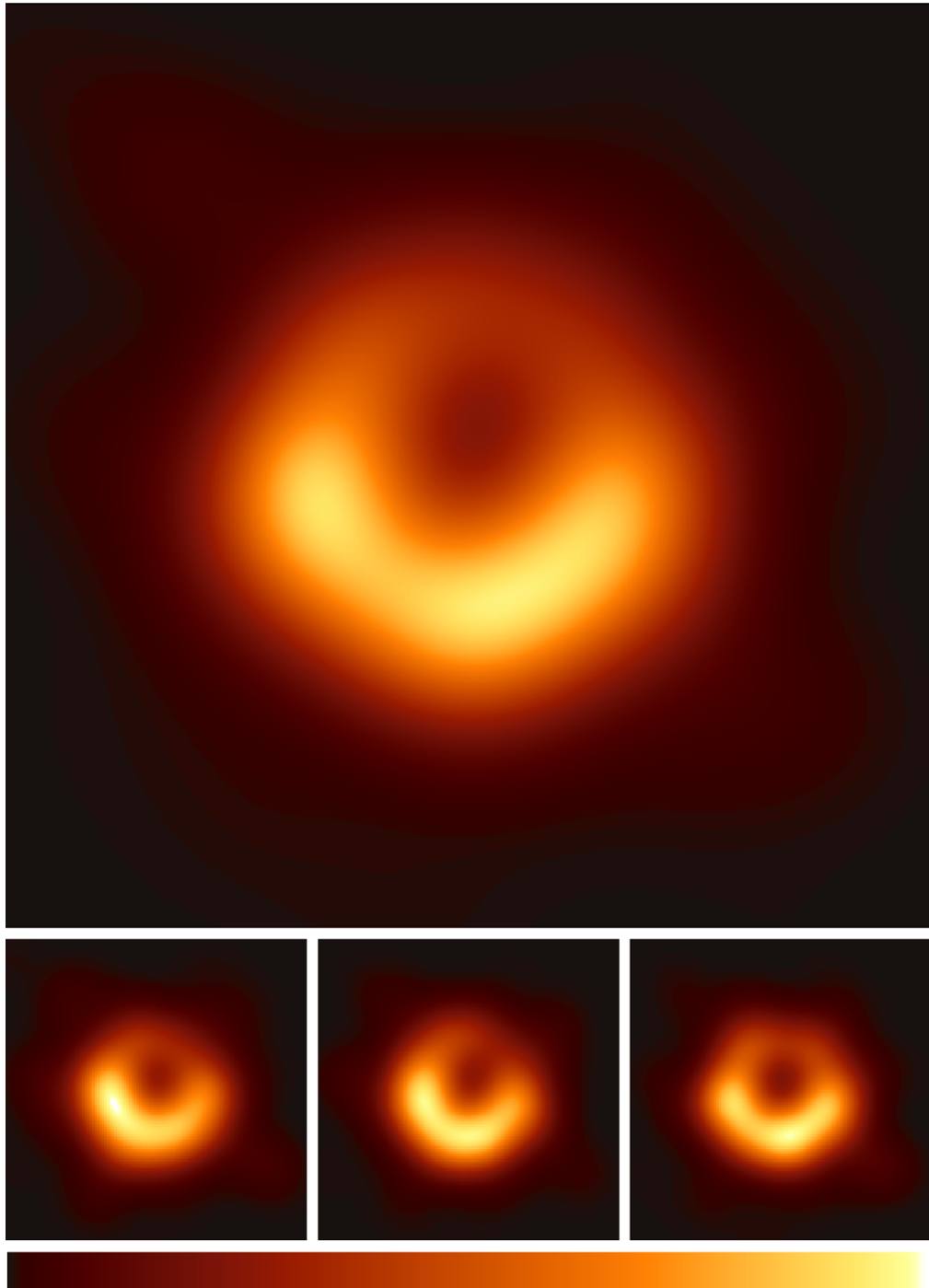


Figure A.1: EHT image of the Supermassive Black Hole in M87 [24].

Black Hole Type	Mass Range	Radius Range (km)
Micro	a few TeV's	—
Stellar	$5M_{\odot}$ — $100M_{\odot}$	15—300
Intermediate-mass	10^2M_{\odot} — 10^5M_{\odot}	300— 3×10^5
Supermassive	10^5M_{\odot} — $10^{10}M_{\odot}$	3×10^5 — 3×10^{10}
Ultramassive	$> 10^{10}M_{\odot}$	$> 3\times 10^{10}$

Table A.1: Classification of black hole by size.

black holes by observing X-ray source of some binary systems [21].

3. **Intermediate-mass black hole** (IMBH) is a kind of black hole with mass range between 10^2M_{\odot} and 10^5M_{\odot} [37]. They are thought to form in the mergers of some stellar black holes [83].
4. **Supermassive black hole** (SMBH) is the largest kind of black hole which have masses ranging between 10^5M_{\odot} and $10^{10}M_{\odot}$. Typically, SMBHs locate at the centers of galaxies (the mass of SMBH at the Galactic Center of Milky Way, Sgr A, is about $4.100 \pm 0.034 \times 10^7M_{\odot}$) [32]. The first black hole image (as shown in Figure.A.1) released on April 10, 2019 by Event Horizon Telescope (EHT) is an image of the supermassive black hole in the center of Messier 87 with mass $6.5 \pm 0.7 \times 10^9M_{\odot}$ [24].

In addition, some researchers also predict the existence of **ultramassive black hole** (UMBH) whose mass should be greater than $10^{10}M_{\odot}$. UMBH may locate at the massive and strong cool cores for some cluster of galaxies [45, 54].

From the above, we can summarize this classification of black holes by size in Table A.1. The ranges used in this table are approximate which may be differed from other papers or textbooks.

A.2 The Solutions of Black Holes

In general relativity, black holes can also be classified according to different solutions to the Einstein field equations with different conditions. These solutions respond to some special behaviors of black holes.

A.2.1 Schwarzschild Black Hole

The Schwarzschild metric is the unique spherically symmetric solution of the vacuum Einstein field equations which can be used to describe the vacuum spacetime outside a spherically symmetric source of curvature (total mass m) in stationary condition [18]. In spherical coordinates (t, r, θ, ϕ) , the Schwarzschild metric is given by [39]

$$ds^2 = -\left(1 - \frac{2m}{r}\right)dt^2 + \left(1 - \frac{2m}{r}\right)^{-1}dr^2 + r^2d\Omega^2, \quad (\text{A.1})$$

where $d\Omega^2 = d\theta^2 + \sin^2\theta d\phi^2$.

It is obvious that there are two singularities at $r = 0$ and $r_s (= 2m)$ in Schwarzschild coordinate. For the coordinate singularity at $r = r_s$, the metric can become regular by changing to some other coordinates, such as Eddington-Finkelstein coordinates, Kruskal-Szekeres coordinates, and Gullstrand-Painlevé coordinates [84]. However, the singularity at $r = 0$ is a real physical singularity for all of those coordinates [15, 84]. The region described by the Schwarzschild spacetime with the radius smaller than r_s

is called Schwarzschild black hole.

The Schwarzschild black hole is the simplest model of black holes without spin and electric charge. Further, this solution is for a black hole in a spacetime without other masses. As such, while they may be good approximation, there are no true Schwarzschild black holes in our universe [84].

For removing the coordinate singularity at $r = r_s$, we can present the Schwarzschild metric in Kruskal coordinates (or Kruskal-Szekeres coordinates) [50]

$$ds^2 = \frac{32m^3}{r} e^{-r/2m} (-dT^2 + dR^2) + r^2 d\Omega^2, \quad (\text{A.2})$$

where

$$T^2 - R^2 = \left(1 - \frac{r}{2m}\right) e^{-r/2m}, \quad (\text{A.3})$$

and

$$\begin{cases} T/R = \tanh(t/2m), & r > 2m, \\ R/T = \tanh(t/2m), & r < 2m. \end{cases} \quad (\text{A.4})$$

In this way, we can obtain the Kruskal diagram (as shown in Figure 2.1 of Section 2.1.1). This process is called the extension of the metric, and the new metric is a maximal extension [18]. In Figure 2.1, the region I is our original universe, and the region IV represents the parallel universe with similar properties to our universe [50, 84]. The region II refers to the Schwarzschild black hole with a future singularity at $r = 0$, and the region III describes the white hole³ with a past singularity at $r = 0$ [84]. The boundary at $r = r_s$ between the region I and region II can be called event horizon which is introduced in Chapter 2.

³On the contrary of black hole, white hole is a region of spacetime where matter or signal can never enter from outside.

In addition, we can also transform the Kruskal diagram to a Penrose diagram (or Carter-Penrose diagram) as shown in Figure A.2 by applying the conformal rescaling of the metric [50, 84]. In this method, we can map the infinite spacetime to a finite portion of the diagram. In the Penrose diagram of Figure A.2, the future and past null infinities are represented as \mathcal{I}^+ and \mathcal{I}^- respectively. The spacelike infinity is i^0 , while the future and past timelike infinity are labelled as i^+ and i^- respectively [61].

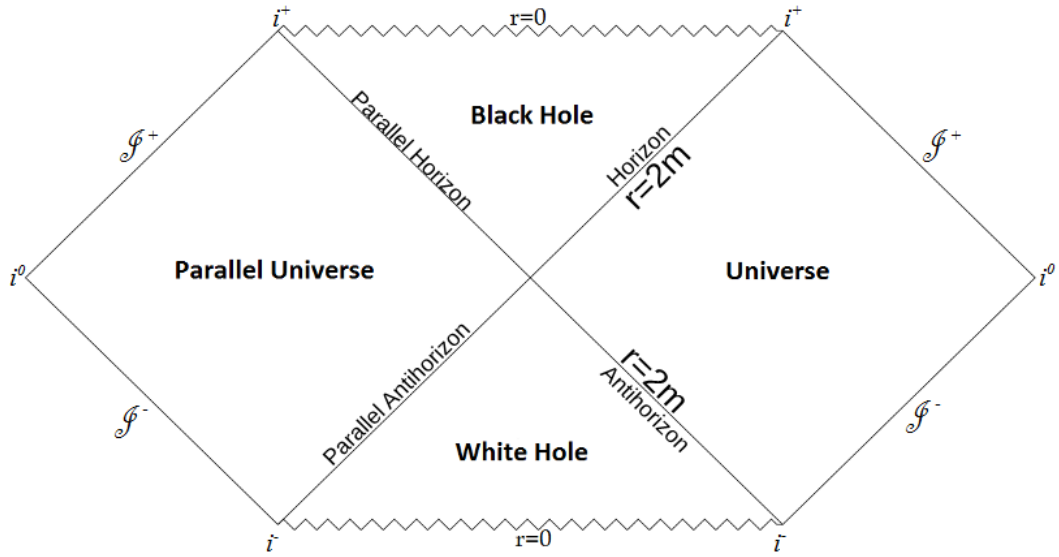


Figure A.2: Penrose diagram of Schwarzschild spacetime. \mathcal{I}^\pm is future/past null infinity, i^0 is spatial infinity, and i^\pm is future/past timelike infinity [61].

Moreover, Schwarzschild metric can also be switch to Eddington-Finkelstein coordinates [39]

$$\begin{cases} ds^2 = -(1 - 2m/r)dv^2 + 2dvdr + r^2d\Omega^2 & \text{(ingoing),} \\ ds^2 = -(1 - 2m/r)du^2 - 2dudr + r^2d\Omega^2 & \text{(outgoing),} \end{cases} \quad (\text{A.5})$$

where

$$\begin{cases} v = t + r + 2m \ln \left| \frac{r-2m}{2m} \right| & \text{(ingoing),} \\ u = t - r - 2m \ln \left| \frac{r-2m}{2m} \right| & \text{(outgoing).} \end{cases} \quad (\text{A.6})$$

If we extend the mass m in (A.5) from constants to functions of (v, u) , the mass function can be transformed to $m(v)$ and $m(u)$, so Schwarzschild metric can become into Vaidya metric which can be used to describe the spherically symmetric spacetime of an object emitting or absorbing dust [61]

$$\begin{cases} ds^2 = -(1 - 2m(v)/r)dv^2 + 2dvdr + r^2d\Omega^2 & \text{(ingoing/advanced),} \\ ds^2 = -(1 - 2m(u)/r)du^2 - 2dudr + r^2d\Omega^2 & \text{(outgoing/retarded).} \end{cases} \quad (\text{A.7})$$

They are solutions for Einstein field equations with stress-energy tensor

$$\begin{cases} T_{\alpha\beta} = \frac{1}{4\pi r^2} \frac{dm}{dv} l_\alpha l_\beta & \text{(ingoing/advanced),} \\ T_{\alpha\beta} = -\frac{1}{4\pi r^2} \frac{dm}{du} l_\alpha l_\beta & \text{(outgoing/retarded),} \end{cases} \quad (\text{A.8})$$

where l_α is tangent to ingoing/outgoing null geodesics.

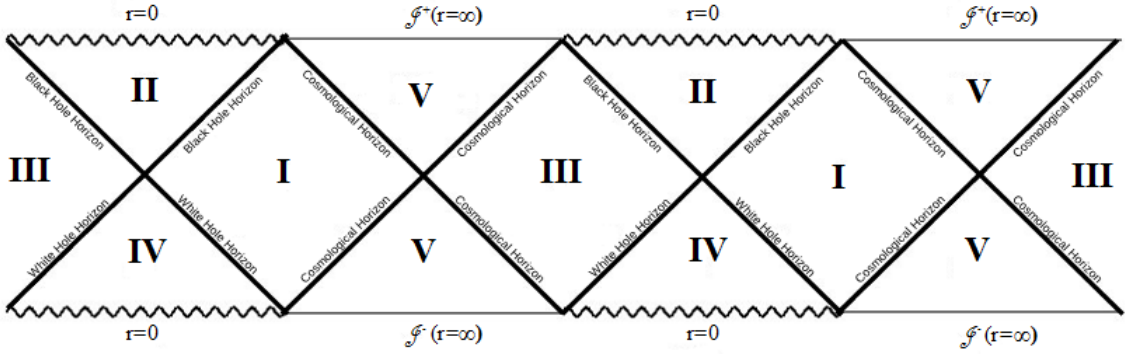


Figure A.3: Penrose diagram of Schwarzschild-de Sitter spacetime. Region I presents our original universe. Region II shows the black hole. Region III describes the white hole. Region IV is the parallel universe. Region V indicates the de Sitter region. \mathcal{I}^\pm is future/past null infinity.

In this thesis, we have investigated the effect of cosmological constant Λ on marginally trapped tube for black hole. So we can extend the Schwarzschild spacetime to Schwarzschild-de Sitter (SdS) spacetime ($\Lambda > 0$) and Schwarzschild-anti-de Sitter (SAdS) spacetime ($\Lambda < 0$) which are also uncharged spherically symmetric solutions to Einstein field equation [2, 72]. In spherical coordinates (t, r, θ, ϕ) , the metric of Schwarzschild- (anti-) de Sitter is given by [16, 72]

$$ds^2 = -\left(1 - \frac{2m}{r} - \frac{\Lambda r^2}{3}\right)dt^2 + \left(1 - \frac{2m}{r} - \frac{\Lambda r^2}{3}\right)^{-1}dr^2 + r^2d\Omega^2, \quad (\text{A.9})$$

where the Λ term is quite similar to the Einstein field equations of Tolman-Bondi-de Sitter spacetime in Chapter 3. Similarly, there are also two event horizons in Schwarzschild-de Sitter spacetime if $0 < y < 1/27$ (where $y = M^2\Lambda/3$) — black hole horizon (r_b) and cosmological horizon (r_c) [16, 69, 72] :

$$\begin{cases} r_b = \frac{1}{\sqrt{3y}} \cos\left(\frac{\pi-\Theta}{3}\right) & (\text{black hole horizon}), \\ r_c = \frac{1}{\sqrt{3y}} \cos\left(\frac{\pi+\Theta}{3}\right) & (\text{cosmological horizon}), \end{cases} \quad (\text{A.10})$$

where $\Theta = \arccos(3\sqrt{3}y)$ and $r_b < r_c$. If $r_b \ll r_c$, the effect of the cosmological horizon on black hole can be ignored, so the situation of Schwarzschild-de Sitter black hole is similar to Schwarzschild black hole [14].

The Penrose diagram of Schwarzschild-de Sitter spacetime is shown in Figure A.3. Comparing with Figure A.2, the Penrose diagram is extended to both sides [15]. In Figure A.3, the region V represents to the de Sitter region in the past or future with the boundary as cosmological horizons [15]. By Equation (A.10), for increasing M and Λ , r_b increases and r_c decreases. When $y = 1/27$ (Nariai limit), the black hole and cosmological horizons coincide corresponding to the Nariai spacetime which is similar to the situations of the examples in Chapter 5 [13, 69].

A.2.2 Kerr Black Hole

The Kerr metric is also a solution to the vacuum Einstein field equations which can be used to describe the spacetime with axisymmetric and stationary conditions [51]. In the standard Boyer-Lindquist coordinates (t, r, θ, ϕ) , the Kerr metric is given by [39]

$$ds^2 = -\frac{\varrho^2 \Delta(r)}{\Sigma} dt^2 + \frac{\Sigma}{\varrho^2} \sin^2 \theta (d\phi^2 - \omega dt)^2 + \frac{\varrho^2}{\Delta(r)} dr^2 + \varrho^2 d\theta^2, \quad (\text{A.11})$$

where

$$\left\{ \begin{array}{l} \varrho^2 = r^2 + a^2 \cos^2 \theta, \\ \Delta(r) = r^2 - 2mr + a^2, \\ \Sigma = (r^2 + a^2)^2 - a^2 \Delta(r) \sin^2 \theta, \\ \omega = 2mar/\Sigma. \end{array} \right. \quad (\text{A.12})$$

The Kerr parameter a is the angular momentum per unit mass $a = J/m$ where J is the angular momentum of black hole. Kerr black hole is a type of uncharged black hole possessing spin. It is obvious that the Kerr metric (A.11) can evolve into Schwarzschild metric while $a = 0$, so a Kerr black hole can also be transformed into a Schwarzschild black hole under this condition [39].

For Kerr black hole, there is a real singularity at $\varrho = 0$ while $r = 0$ and $\theta = \pi/2$ [51]. And for $\Delta = 0$, there are two coordinate singularities at $r_{\pm} = m \pm \sqrt{m^2 - a^2}$ [51]. Hence, there are two event horizons for Kerr black hole: the outer and inner horizons which are the null, axisymmetric and stationary three-surfaces with radii $r = r_{\pm}$ respectively [18, 39]. The region outside the outer event horizon is called ergosphere (except at poles $\theta = 0$ and π) which holds the rotational energy of the black hole [39, 50]. The outer boundary of ergosphere is known as static surface where

the $g_{tt} = 0$ and the radius [39]

$$r_e(\theta) = M + \sqrt{M^2 - a^2 \cos^2 \theta}. \quad (\text{A.13})$$

The Kerr metric can be extended to the Kerr-Newman metric by including electric charges. In this way, the new $\Delta(r)$ changes into

$$\Delta(r) = r^2 - 2mr + a^2 + Q^2, \quad (\text{A.14})$$

where Q is the total electric charge of black hole [50, 51]. Therefore, the radii of the outer and inner event horizons have developed into $r_{\pm} = m \pm \sqrt{m^2 - a^2 - Q^2}$ [15]. Hence, the Kerr-Newman black hole is also known as the charged black hole with spin [1].

Similar to the Schwarzschild spacetime of Appendix A.2.1, Kerr spacetime can also be extended to the Kerr-de Sitter spacetime and Kerr-anti-de Sitter spacetime with the positive and negative cosmological constants respectively [2, 73]. In the standard Boyer-Lindquist coordinates (t, r, θ, ϕ) , the Kerr- (anti-) de Sitter metric is as follows [73]

$$ds^2 = -\frac{\Delta_r}{I^2 \varrho^2} (dt - a \sin^2 \theta d\phi)^2 + \frac{\Delta_{\theta} \sin^2 \theta}{I^2 \varrho^2} [adt + (r^2 + a^2)d\phi]^2 + \frac{\varrho^2}{\Delta_r} dr^2 + \frac{\varrho^2}{\Delta_{\theta}} d\theta^2, \quad (\text{A.15})$$

where

$$\begin{cases} \Delta_r = r^2 - 2mr + a^2 - \Lambda r^2(r^2 + a^2)/3, \\ \Delta_{\theta} = 1 + (\Lambda a^2 \cos^2 \theta)/3, \\ I = 1 + \Lambda a^2/3. \end{cases} \quad (\text{A.16})$$

Similarly, we can also introduce the Kerr-Newman (anti-) de Sitter spacetime by the new Δ_r with Q

$$\Delta_r = r^2 - 2mr + a^2 - \Lambda r^2(r^2 + a^2)/3 + Q^2. \quad (\text{A.17})$$

Moreover, in the Kerr-Newman de Sitter spacetime, the outer black hole event horizon and the cosmological horizon can coincide each other with the Nariai limit [12].

A.2.3 Reissner-Nordström Black Hole

The Reissner-Nordström metric is a solution to the Einstein-Maxwell field equations which can be used to describe the vacuum spacetime outside a static, charged, spherically symmetric body with mass m . The Reissner-Nordström metric in spherical coordinates (t, r, θ, ϕ) is given by [61]

$$ds^2 = -\left(1 - \frac{2m}{r} + \frac{Q^2}{r^2}\right)dt^2 + \left(1 - \frac{2m}{r} + \frac{Q^2}{r^2}\right)^{-1}dr^2 + r^2d\Omega^2, \quad (\text{A.18})$$

where $d\Omega^2 = d\theta^2 + \sin^2\theta d\phi^2$, and Q is the total electric charge of the body. In this case, Reissner-Nordström black hole is known as another charged black hole which is non-rotating (by contrast with the Kerr-Newman black hole), so Reissner-Nordström black hole can become into Kerr-Newman black hole by including rotation. In addition, Reissner-Nordström black hole can also reduce to Schwarzschild black hole while the total charge $Q = 0$.

The features of Reissner-Nordström metric are associated with the relationship between m and Q . In Reissner-Nordström spacetime, there is a real singularity at $r = 0$ similar to Schwarzschild spacetime. By considering the element of the metric g_{rr} , we have $1 - 2m/r + Q^2/r^2 = 0$ at $r_{\pm} = m \pm \sqrt{m^2 - Q^2}$ [15, 18]

1. $m^2 < Q^2$: There is no event horizon. The real singularity at $r = 0$ has become a naked singularity.
2. $m^2 > Q^2$: The metric has two coordinate singularities at $r = r_{\pm}$ and one real

singularity at $r = 0$. The surface $r = r_+$ is called outer horizon, and the surface $r = r_-$ is inner horizon (internal Cauchy horizon).

3. $m^2 = Q^2$: There is only one coordinate singularity at $r = m$. The black hole with the event horizon at $r = m$ is known as an extremal Reissner-Nordström black hole.

Besides, the Reissner-Nordström spacetime can also become a Reissner-Nordström-(anti-) de Sitter spacetime with positive and negative cosmological constants respectively [2]. The metric of Reissner-Nordström-(anti-) de Sitter spacetime is given by [2]

$$ds^2 = -\left(1 - \frac{2m}{r} + \frac{Q^2}{r^2} - \frac{\Lambda r^2}{3}\right)dt^2 + \left(1 - \frac{2m}{r} + \frac{Q^2}{r^2} - \frac{\Lambda r^2}{3}\right)^{-1}dr^2 + r^2d\Omega^2. \quad (\text{A.19})$$

A.2.4 Summary

Ultimately, we can obtain Table A.2 of black hole by summarizing the previous sections. In Table A.2, the black holes are sorted according to angular momentum J and electric charge Q .

Black Hole Type	Angular Momentum J	Electric Charge Q
Schwarzschild	$J = 0$	$Q = 0$
Kerr	$J > 0$	$Q = 0$
Kerr-Newman	$J > 0$	$Q \neq 0$
Reissner-Nordström	$J = 0$	$Q \neq 0$

Table A.2: Classification of stationary black hole solutions of the Einstein-Maxwell equations by angular momentum and electric charge.